Visualization of interactions between chemoautotrophic symbionts and gill epithelial cells of *Thyasira* cf. *gouldi* using confocal microscopy and transmission electron microscopy

Kiana Marie Alfaro, B.Sc.

A thesis submitted to the School of Graduate Studies in partial fulfillment of the requirements for the degree of

Master of Science

Department of Biology
Memorial University of Newfoundland

April 2024

Abstract

Many species of marine clams from the family Thyasiridae form symbioses with sulfur oxidizing bacteria, which are maintained externally on gill epithelial cells. Transmission electron microscope images suggest that host cells phagocytose and lyse symbionts to obtain nutrients. However, as this technique can only reveal two-dimensional sections of cells, interactions between host and symbionts, particularly with regards to phagocytosis and lysis, remain incompletely characterized. Here, fluorescent labelling and confocal microscopy of *Thyasira* cf. *gouldi* gills are used to visualize host nuclei, actin, acidic organelles, and symbiotic bacteria. I found that DAPI stained host nuclei but not symbionts. Actin labelling using phalloidin labeled microvilli but did not show obvious phagocytotic structures. The combined use of LysoTracker and CTC to label acidic organelles and symbionts, respectively, proved problematic due to colocalization, but labelling suggested low numbers of acidic organelles (lysosomes) and active symbionts. Results obtained, along with a review of transmission electron microscope images of *T*. cf. *gouldi* gill cells, suggest that nutrient transfer pathways may involve more morphologically complex structures and potentially different processes than previously thought. In future work, single gill cells should be reconstructed using FIB-SEM to visualize host cellular structures and symbiont cells in three dimensions.

Keywords: confocal, fluorescence microscopy, bivalve, Newfoundland, chemosymbiosis

Acknowledgements

I have endless thanks to Dr. Suzanne Dufour, my supervisor, for her endless support and for believing in me when I did not believe in myself. I would not have been able to do this without her and having her in my corner when I needed it. Thank you to my lab for the helpful comments and suggestions.

Thank you to my committee members, Dr. Helene Volkoff and Dr. Andrew Lang for all the advice and understanding with my ever-changing chapters. Andrew, I am sorry for losing your cat - but we got her back!

To the Bonne Bay field station, thank you for helping me get my clam babies! You all were always so accommodating and helpful, even when we did all that to get a single clam. I would like to express my gratitude to Stephanie and Nick at the Electron Microscopy lab in the Health Science Center for training me on the ultramicrotome, confocal microscope and transmission electron microscope. A special thank you to Valentin Kokarev, a postdoc in the Dufour lab for helping me out with my maps.

I cannot thank my parents, Penny and Robert, and my brother, John, enough for pushing me to do my best and to keep going even when I swear I could not. Without them, I definitely would not be where I am today - and not just physically. Although, I am pretty sure they still do not know what I'm talking about.

To my long-distance best friend, Alysha - thank you for believing in me, encouraging me to do my best and threatening me out of my imposter syndrome. After submitting this, I could finally join in on all the trips. Thank you to Johanna Bosch for being an amazing friend and always being there to help me out. Special thanks to Amber Walker for keeping me well fed and getting me into embroidery. Finally, a huge thank you to my entire heart, my sweet baby Beans.

I would like to respectfully acknowledge the territory in which this study took place as the ancestral homelands of the Beothuk, and the island of Newfoundland as the ancestral homelands of the Mi'kmaq and Beothuk.

Table of Contents

List of Tables

List of Figures

List of Abbreviations

cf.	confer
CTC	5-cyano-2,3-di-(p-tolyl)-tetrazolium chloride
DAPI	4′,6-diamidino-2-phenylindole
FIB-SEM	focused ion beam – scanning electron microscope
Ly	lysosome
mv	microvilli
mw	membrane whorl
n	nuclei
PBS	phosphate buffered saline
PI	propidium iodide
RLO	*Rickettsia*-like organisms
rRNA	ribosomal RNA
TEM	transmission electron microscope
SUP05	sulfur oxidizing bacteria

List of Appendices

Chapter 1: Introduction and Thesis overview

Animals may interact with bacteria in many ways, including through a type of beneficial interaction called chemosymbiosis, first discovered at deep-sea hydrothermal vents just over 40 years ago. Chemosymbioses are relationships between animal hosts and bacterial symbionts where symbionts gain energy by oxidizing reduced sulfide, methane or hydrogen and fix carbon dioxide and other small carbon compounds, providing the host as well as themselves with nutrition (Petersen et al., 2011). While the hosts span many taxonomic groups, characterized chemosynthetic symbionts that have been shown to provide nutrients to their host belong to the class Gammaproteobacteria; most hosts associate with only one or a few symbiont species or strains (Sogin et al., 2020, 2021). Chemosymbiotic relationships are not restricted to deep-sea hydrothermal vents, and have been documented from many marine habitats including cold seeps, whale and wood falls, shallow water and continental slope sediments (Dubilier et al., 2008). In many cases, chemosymbiosis allows the hosts to live in environments where a strict heterotrophic diet may not be supported (Sogin et al., 2020).

1.1. Chemosymbiosis in Bivalves

Chemosymbiosis has been a highly successful strategy in the bivalve molluscs: over 600 species of bivalves have been described as chemosymbiotic, across a broad range of habitats (Hughes & Giurguis, 2023). The bivalve families that have been demonstrated to form chemosymbiotic relationships are the Lucinidae, Thyasiridae, Solemyidae, Vesicomyidae, Teredinidae and Mytilidae, with most of the recorded symbionts consisting of gammaproteobacteria (Sogin et al., 2021). Bivalve chemosymbioses are diverse in many ways: for example, the degree of nutritional reliance of bivalves upon their symbionts, the metabolic

repertoire of these symbionts, and the ways in which host and symbiont interact with each other vary across families. In the Lucinidae, which is the most species-rich family of chemosymbiotic bivalves (Taylor & Glover, 2010), all species examined are obligately chemosymbiotic and harbour sulfur-oxidizing symbionts, which in some instances may additionally fix nitrogen (König et al., 2016; Petersen et al., 2016). In the Thyasiridae, some species are chemosymbiotic and derive part of their nutritional requirements from their symbionts, while other species lack symbionts altogether (Zanzerl et al., 2019). Described thyasirid symbionts are sulfur-oxidizing gammaproteobacteria from the Family Sedimenticolaceae or the SUP05 clade (Sogin et al., 2021). The Solemyidae mostly supplement sulfur-oxidizing symbiont-derived nutrition with heterotrophic feeding, with the exception of *Solemya reidi,* which is gutless and cannot suspension feed as an adult (Powell & Somero, 1985). The Vesicomyidae are usually found at hydrothermal vents and all studied species host sulfur-oxidizing chemosymbionts (Hughes & Guirguis, 2023). Teredinidae (shipworms) are mainly known for breaking down wood with the assistance of their cellulase-producing bacterial symbionts (Hughes & Giurguis, 2023); recently, the giant shipworm *Kuphus polythalamius* was found in sulfidic sediments, harbouring sulfur-oxidizing chemoautotrophic symbionts (Shipway et al., 2018). FISH and confocal microscopy have been used effectively in studying symbiosis in Teredinidae (Altamia & Distel, 2022; Betcher et al., 2012). In the Mytilidae, members of the subfamily Bathymodiolinae may host symbionts with various chemolithotrophic metabolic pathways, including methanotrophy and hydrogen oxidation (Petersen et al., 2011). Individuals of *Bathymodiolus* can host multiple strains of symbionts that use different energy sources (Ansorge et al., 2019).

Chemosymbiotic bacteria typically colonize specific host tissues (Hentschel et al., 2000); in bivalves, symbionts are generally restricted to gills (at least in adults), where they are

associated with epithelial cells called bacteriocytes (Wentrup et al., 2013). Bivalve symbionts are either intracellular or extracellular, depending on the host species; most research has focused on intracellular symbioses, which represent the more integrated and co-dependent state. In lucinids (e.g. *Anodontia philippiana*, *Lucina multilineata, L. radians,* and *L. costata),* the symbionts are located intracellularly, with each bacterium housed within its own vacuole (Giere, 1985). Four morphotypes of mytilids examined by transmission electron microscopy (TEM) maintained bacteria extracellularly, between the microvilli at the apical surface of cells along the lateral zone of the gill filaments (Gros & Gaill, 2007) while symbionts in other mytilids are intracellular (Childress et al., 1986). In most symbiotic thyasirids, symbionts are maintained extracellularly between a thin cuticle and the apical membrane of host gill cells (Southward, 1986) while in one thyasirid species, symbionts are described as intracellular, with large numbers of them being grouped in large vacuoles (Fujiwara et al., 2001). A possible advantage of hosting intracellular symbionts may be that it enables a more direct access to readily available nutrients compared to extracellular symbionts.

1.1.1 Nutrient transfer in chemosymbiotic bivalves

By pumping seawater through their gills, chemosymbiotic bivalves provision their bacterial symbionts with resources such as reduced sulfur and oxygen, and in turn receive products from their symbionts through 'milking' or 'farming' pathways (Sorgin et al., 2020). Hosts that 'milk' their symbionts keep them alive and receive organic carbon and other nutrients via direct transfer, presumably through bacterial excretion, secretion, or vesicular transport (Sorgin et al., 2020; Wang et al., 2023). Symbionts that are 'farmed' are maintained alive for some time and are eventually digested intracellularly by host lysosomes; this process is

considered common among chemosymbioses (Sorgin et al., 2020), including in species with extracellular symbionts (e.g. the Thyasiridae, Laurich et al., 2015).

1.1.1.1 Direct transfer (milking)

Milking is a possible pathway for nutrient uptake by chemoautotrophic hosts where symbionts remain alive and directly transfer small molecules such as sugars and amino acids to the host. There is currently little support for milking as the predominant mode of nutrient transfer in chemosymbiotic hosts, given that carbon transfer is difficult to trace and hosts need other nutrients besides carbon (Sogin et al., 2021). While milking is a likely feature of some intracellular symbioses, it has yet to be confirmed in extracellular symbioses, where membrane transporters might be required for bacteriocytes to efficiently take up products secreted by symbionts.

1.1.1.2 Symbiont digestion (farming)

The intracellular digestion of symbionts (farming) likely occurs in all chemosymbiotic bivalves, including in species that use the milking strategy, as it can help control symbiont population size in addition to providing the host with nutrients (Le Pennec et al., 1988; Laurich et al., 2018). In bivalves with extracellular symbionts, the expected pathway for nutrient transfer involves a sequential process of phagocytosis, phagolysosome production, and lysosomal degradation (Fig. 1).

Phagocytosis is a process of food uptake and defence against pathogens in eukaryotes (Weiss & Shaible, 2015). Through this process, a particle present in the extracellular matrix is engulfed and transported into the cell using actin cytoskeletal filaments in the plasma membrane

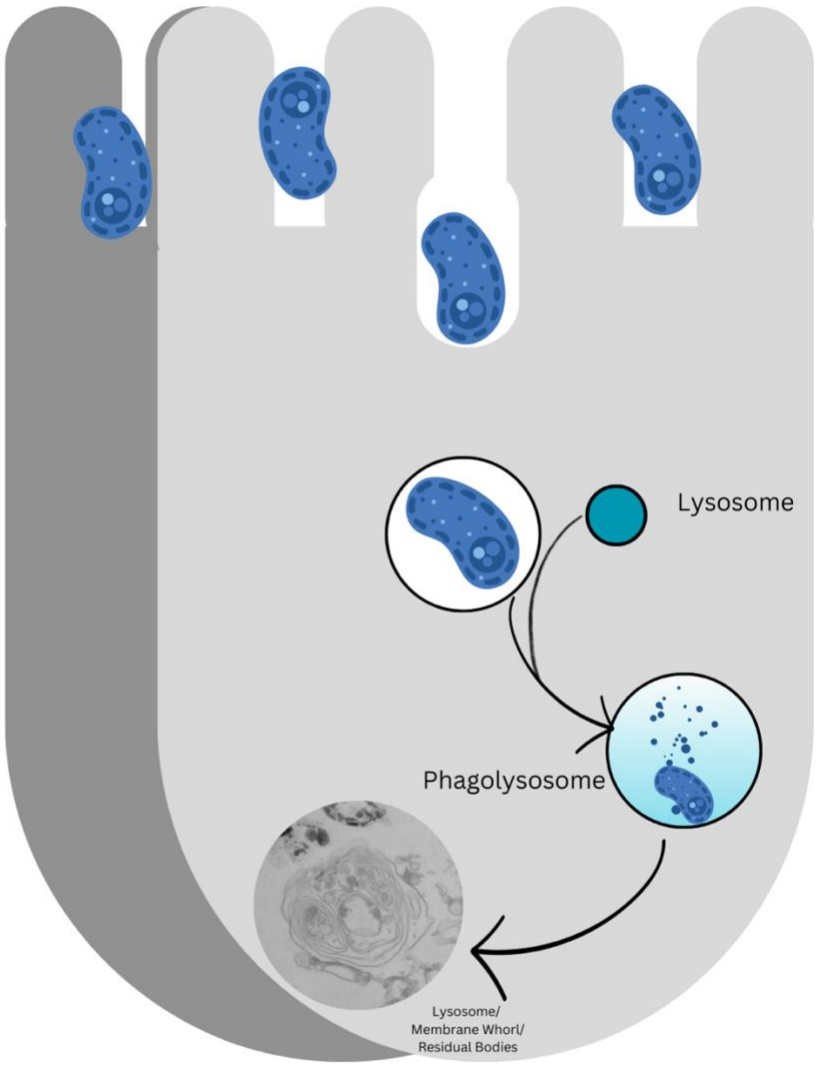

Figure 1: Diagram illustrating the phagocytosis and degradation of extracellular symbiotic bacteria in a bivalve bacteriocyte. Diagram generated using Canva.

(Deshpande & Wadhwa, 2023). After the particle has been engulfed, it is compartmentalized in an intracellular vesicle called a phagosome (Fig. 1). In bivalves with extracellular symbionts such as thyasirids and some bathymodiolins, phagocytosis may be an essential process for nutrient acquisition. Phagocytosis is a means for hosts to acquire intracellular symbionts from the environment (Bright & Bulgheresi, 2010); for hosts to maintain intracellular symbionts without digesting them requires the regulation or suppression of lysosomal activity and immune responses through processes that are not yet understood (Li et al., 2023a).

Visual evidence for symbiont phagocytosis in bivalves has been obtained through observation of bacteriocytes using TEM. For example, Le Pennec et al. (1988) recorded endocytosis of bacteria in the gills of *Bathymodiolus thermophilus, Thyasira flexuosa* and *Lucinella divaricata* by observing host-cell vacuoles in cross-sections of bacteriocytes. More recently, transcriptome analysis showed that genes involved in phagocytosis were highly expressed in bacteriocytes of the seep-dwelling *Thyasira* sp. Haima (a species in which the intracellular or extracellular location of symbionts is not known), suggesting evidence of active symbiont phagocytosis (Li et al., 2023b). In bivalves with extracellular symbionts, the rate at which symbionts are being phagocytosed may not always be constant. Possible triggers for symbiont phagocytosis might include symbiont abundance, availability of alternate food resources, and the physiological/reproductive state of the host (Laurich et al., 2015; Tame et al., 2023).

After a phagosome is formed, it then fuses with one or more lysosomes to become a phagolysosome (Fig. 1), in which microorganisms can be digested (Deshpande & Wadhwa, 2023). The pH in a phagolysosome is ~4.5 due to the hydrolytic enzymes such as cathepsins, proteases, lysozymes and lipases that enable the degradation of phagocytosed microorganisms

(Cooper, 2000; Uribe-Querol & Rosales, 2020). In gills of *Thyasira* sp. Haima, highly expressed calreticulin (which recruits lysosomes to phagosomes), V-type H+-transporting ATPase (which lowers the pH in phagolysosomes) and cathepsins were identified as markers of symbiont digestion (Li et al., 2023b).

TEM-based observations of concentric "onion peel" structures, typically located toward the basal end of bacteriocytes, have been interpreted as evidence of lysosomal degradation in bivalves (e.g. Piquet et al., 2022). It has been assumed that after lysosomal degradation of the bacterial symbionts, the remains form what have been called 'membrane whorls' (Le Pennec et al., 1988; Passos et al., 2007), or 'residual bodies' (Kádár et al., 2008). These appear as pigmented, granular, myelin-like structures (Le Pennec et al., 1988) that have an elemental composition that is similar to that of symbionts (Kádár et al., 2008). TEM imaging indicates that there may be many membrane whorls in each bacteriocyte, and that they may be as large as the nucleus and occupy a considerable amount of space in the cytoplasm (Passos et al., 2007).

Membrane whorls have been observed within bacteriocytes of bivalves with extracellular symbionts (e.g. *Thyasira* cf. *gouldi, Thyasira flexuosa*; Le Pennec et al., 1988; Laurich et al., 2015) as well as species with intracellular symbionts (e.g. *Bathymodiolus azoricus*; Piquet et al., 2022). Kádár et al. (2008) used enzyme cytochemistry along with X-ray microanalysis and electron microscopy to study lysosomal digestion in bacteriocytes of the vent mussel *Bathymodiolus azoricus*. Among the structures they identified as residual bodies (i.e. large cellular inclusions with membranous content), a small number showed weak evidence of acid phosphatase activity (Kádár et al., 2008). The apparently low incidence of symbiont digestion through lysosomal activity in *B. azoricus* bacteriocytes was thought to be due to the majority of nutrient transfer being through milking in this species, with symbiont digestion being mainly a

result of bacterial autolysis. Attempts to detect hydrolase enzymes in the membrane whorls of gill bacteriocytes in other mussels and lucinids showed a similarly low and inconsistent enzymatic activity (Streams et al., 1997; Liberge et al., 2001), suggesting that these structures may represent a late, post-catabolic stage of bacterial digestion (Kádár et al., 2008).

Although membrane whorls appear to be common and relatively consistent features of bacteriocytes in some bivalve species, the nature of these structures and their potential usefulness as indicators of symbiont digestion remain uncertain. It is not clear whether membrane whorls represent a range of catabolic stages in the host cell, or how they change over time. Rather than consisting of packaged remnants of symbiont cell membranes (which are likely readily digestible by host cells), they might consist of more resistant peptidoglycan, which are large, sac-like, rigid polymers that form scaffolds as part of bacterial cell walls (Garde et al., 2021) that may be difficult for host cells to degrade. The longevity and fate of membrane whorls, as well as the impact of buildup of these structures in bacteriocytes, are unknown.

1.1.2 Symbiont state and bacteriocyte housekeeping

At a given time, populations of symbionts associated with a bivalve host may include individuals that are active and others that are inactive, or even dead. The condition of symbionts could be impacted by concentrations of metabolites in their immediate environment (Laurich et al., 2018), under the influence of factors including the host bivalve's irrigation behaviours (which transport water from the outside environment to the inner mantle cavity), the transport of metabolites in the bivalve's circulatory system (e.g. oxygen transported on vesicomyid hemoglobin; Decker et al., 2017), and external conditions. Symbionts that are dead or dying may undergo autolysis, as suggested for intracellular symbionts of *Bathymodiolus azoricus* following

transport from deep sea vents to the surface (Kádár et al., 2008). Hosts that are not receiving nutrients from symbionts may be triggered to lyse those bacteria as a form of housekeeping (Tame et al., 2022, 2023; Wang et al., 2023). A more complete understanding of host-symbiont interactions and energetics in chemosymbiotic bivalves requires considering the condition and physiology of both bacteria and bivalves.

1.2 Thyasirids as models of extracellular chemosymbiosis

The family Thyasiridae includes 25 genera and approximately 120 described recent species (MolluscaBase, 2024), and has a fossil record dating back to the Lower Jurassic period (Karapunar et al., 2020). Thyasirids are found worldwide in cold marine sediments, from shallow coastlines at high latitudes to abyssal depths, occupying various habitats including cold seeps and some hydrothermal vents (Keuning et al., 2011). Some (but not all) species of thyasirids form symbioses with sulfur oxidizing bacteria; stable isotope work indicates that symbiotic thyasirids rely less on nutrients obtained from their symbionts than do other chemosymbiotic bivalves (Dando & Spiro, 1993). In all but one symbiotic species, the symbionts are extracellular and maintained among microvilli of bacteriocytes (Keuning et al., 2011). Gill anatomy varies within the family, with asymbiotic species having simple, "type 1" (Dufour, 2005) gill filaments that are not abfrontally elongated, while symbiotic species have filaments with greater fusion ("type 2", Dufour, 2005) or abfrontal expansion ("type 3", Dufour, 2005), sometimes with further structural modifications (Oliver, 2014). Symbiotic thyasirids have been proposed to represent early stages of the evolution of chemosymbiosis because of the extracellular location of their symbionts (Dufour, 2005).

Feeding strategies vary among species of thyasirids, including both symbiotic and asymbiotic species. Symbiotic thyasirids use their foot to burrow into the surrounding sediments to access reduced sulfur for the sulfur-oxidizing bacteria in their gills (Zanzerl & Dufour, 2018). A mixotrophic diet – relying on nutrients from symbionts and from particulate organic matter obtained by suspension feeding or pedal feeding (Zanzerl et al., 2019) – was suggested for symbiotic thyasirids, with the contribution from symbionts varying across years (Dando & Spiro, 1993). Symbiotic thyasirids are often larger than asymbiotic species, and this size difference may be due to the symbiotic thyasirids having a greater overall nutritional input (Dufour, 2005). Dynamic energy budget models suggest that maintaining symbionts leads to physiological differences in energy allocation to reserves, somatic maintenance, growth rates, maturity and reproduction in thyasirids (Mariño et al., 2019).

Perhaps due to their small size (most measure < 1 cm), there has been relatively less focus on chemosymbiosis in thyasirids than on other bivalve families; however, continued research on certain model taxa, such as *Thyasira* cf. *gouldi* from fjords in Newfoundland, has provided new insights on host-symbiont specificity (Batstone & Dufour, 2016), behaviour (Zanzerl & Dufour, 2018) and evolution (Batstone et al., 2014) in a bivalve with extracellular symbionts.

1.2.1 *Thyasira* cf. *gouldi*

Thyasira gouldi was first described from individuals collected from deep water off Massachusetts, USA (Philippi,1845). The species has been reported from sites throughout the Arctic and Subarctic, usually in clay sediments that are organically enriched at < 50 m depth (Batstone et al., 2014). Specimens collected from the subarctic fjord of Bonne Bay,

Newfoundland, Canada, resemble *T. gouldi* from the type location. However, based on sequencing of the 18S and 28S rRNA gene, they were found to form a complex of 3 closely related operational taxonomic units (OTUs), with only types 1 and 2 being symbiotic (Batstone et al., 2014). Here, I focus on the symbiotic OTUs, referring to them as *Thyasira* cf. *gouldi* as has been the practice in other studies of the Bonne Bay specimens (Batstone et al., 2014). The "cf." designation recognizes that there is likely a species complex within the broadly defined "*Thyasira gouldi*" taxon, and that it remains uncertain whether the specimens from Bonne Bay belong to the same species as the type specimen of *T. gouldi* collected from off Massachusetts.

Symbiotic *Thyasira* cf. *gouldi* were described to have gill type 3 of Dufour (2005), with two demibranchs (Fig. 2A, B) and abfrontally expanded gill filaments with a distinct bacteriocyte zone (Fig. 2C). The frontal surface of the gill is ciliated, but not the bacteriocyte zone (Fig. 2C). The bacteriocytes have microvilli (Fig. 2D) which enclose symbionts within a space that can appear large relative to the bacteriocyte's cytoplasm, as in other thyasirids (Dufour, 2005). The symbionts of *T.* cf. *gouldi* are elongated rods (Batstone et al., 2014) that can measure several µm in length. Symbionts appearing to be actively dividing have been observed in the gills of *T.* cf. *gouldi* (Laurich et al., 2018).

The interactions between *Thyasira* cf. *gouldi* and their symbionts are poorly understood. Three strains of sulfur-oxidizing gammaproteobacteria have been documented in the gills of *T.* cf. *gouldi* from Bonne Bay (Batstone et al., 2014), including within the gills of individual hosts (McCuaig et al., 2017). The mixture of strains in a host individual can be due to the symbionts being picked up from sediment microbial communities and retained extracellularly on the gills (McCuaig at al., 2017) rather than transmitted vertically through eggs as in other chemosymbiotic hosts. Nutritional inputs from symbionts to thyasirid hosts can differ across

individuals and sampling dates (Zanzerl et al., 2019) and appear to occur through endocytosis of the symbionts, which are lysed in the host cell, resulting in membrane whorls (Laurich et al., 2015). Examinations of the gills of *T.* cf. *gouldi* using TEM have revealed that the abundance of symbionts (estimated by measuring percent spatial occupation of symbionts in bacteriocytes on ultra-thin gill sections) varies according to a seasonal pattern, with abundance being highest in the fall and lowest in the spring (Laurich et al., 2015). Membrane whorls were observed in those same bivalves, and their spatial occupation quantified as a potential indicator of symbiont digestion rate. Intriguingly, the spatial occupation of membrane whorls did not seem to show a similar temporal pattern as observed for symbiont spatial occupation (Laurich et al., 2015). The factors underlying the dynamics of symbiont abundance in *T.* cf. *gouldi* have not been established, but the abundance of symbionts at a particular time is likely the result of (some combination of): 1) the abundance of free-living symbionts in surrounding sediments; 2) the rate of symbiont uptake from the environment; 3) the rate of symbiont division at the surface of gills; and 4) the rate of symbiont phagocytosis by host gill cells. It is not known if phagocytosis might be triggered by inactivity or death of symbionts in the extracellular space (a form of housekeeping), and/or host "hunger" state (Li et al., 2023b; Wang et al., 2023).

Current understanding of symbiont phagocytosis by thyasirid gill epithelial cells and of the intracellular digestion of these symbionts is restricted to information that can be obtained from ultra-thin (70 nm thick) sections of cells observed via TEM. As TEM imaging reveals two-dimensional sections of cells, events such as phagocytosis are only captured when the plane of sectioning is in alignment with endocytotic structures. Therefore, TEM likely underestimates the prevalence of phagocytosis events within individual cells. Additionally, thin sections are unlikely to reveal connections between membrane whorls and phagosomes, or whether larger membrane

whorls are the result of the fusion of many smaller structures. To better understand the fine structure and temporal dynamics of symbiont phagocytosis and lysis, other tools are required.

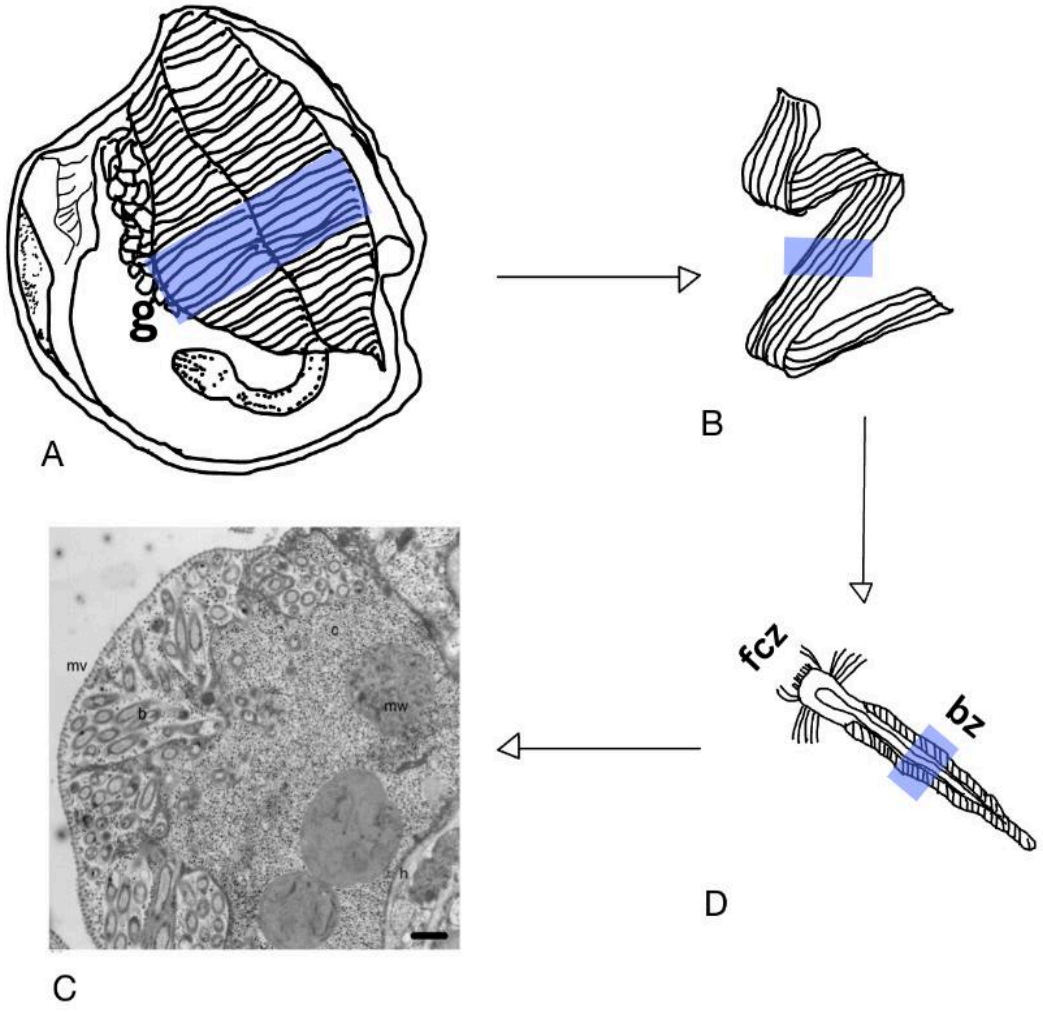

Figure 2. Schematics of thyasirid gills and representation of a bacteriocyte as viewed using transmission electron microscopy. Schematic produced using Notability and Canva. **(A)** Internal anatomy of a symbiotic thyasirid showing prominent gills (g). The blue area shows a segment of two demibranchs, shown in **(B)** to be made up of rows of individual, V-shaped filaments, which after embedding and sectioning, appear as single gill filaments **(C)** with a frontal ciliated zone

(fcz) and bacteriocyte zone (bz). **(D)** Transmission electron micrograph of a bacteriocyte, showing the cytoplasm (c), microvilli (mv), hemocoel (h), and bacteria (b).

1.3 Gill imaging through Confocal Laser Microscopy

Confocal microscopy could provide us with a different perspective of thyasirid bacteriocytes than what is currently obtained from TEM imaging of single, non-consecutive, ultra-thin sections. Confocal microscopes use a laser beam, tunable to specific wavelengths and focused through a pinhole, to scan an object along successive sectioning planes. An image is produced, pixel by pixel, by collecting emitted photons from fluorophores (fluorescent labels) in the sample (Collazo et al., 2005).

Confocal microscopy gives us an opportunity to look at thyasirid gills as whole mounts (without requiring gills to be embedded or cut using an ultramicrotome, thus saving processing time), using optical sectioning to observe bacteriocytes along single planes and stacks of consecutive sections. In addition, fluorescent stains can be selected and used in various combinations to target cellular components or features such as live/dead symbiont state or active lysosomal degradation, which are not readily observed using TEM.

1.3.1 CTC (5-cyano-2,3-ditolyl tetrazolium chloride)

5-cyano-2,3-di-(p-tolyl)-tetrazolium chloride (CTC) is a live/dead redox dye used to visualize bacteria undergoing respiration that is colorless as a salt powder. CTC is reduced by the electron transport activity of the respiring bacteria to form CTC-formazan which then becomes fluorescent (Rodriguez et al., 1992). CTC was used to label active respiring bacteria for enumeration on a natural stone in combination with a confocal laser scanning microscope (Bartosch et al., 2003). Here, I use CTC to label actively respiring *T*. cf. *gouldi* symbionts, which

could provide an indication of the proportion of the symbiont population that is active on the gills, as well as reveal any differences in activity level according to spatial location on the gills.

1.3.2 Propidium Iodide

Propidium iodide (PI) is a membrane impermeable stain that binds to DNA and RNA. It is used to test bacterial viability as it only enters bacteria with damaged membranes, staining them red (Boulus et al., 1999). Propidium iodide is usually used in combination with a membrane permeable counterstain (Rosenburg et al., 2019). Here, we use propidium iodide to attempt to visualize dead/inactive symbionts in *T.* cf. *gouldi* bacteriocytes. Having the ability to visualize dead symbionts could provide basic information on the health of symbiont populations on a gill. Additionally, labelling of dead symbionts could reveal whether they are preferentially phagocytosed by host cells as a form of housekeeping.

1.3.3 DAPI (4′,6-diamidino-2-phenylindole)

4′,6-diamidino-2-phenylindole (DAPI) is a membrane impermeable, blue fluorescent probe which binds specifically to A-T rich sequences of DNA (Kapuscinski, 1995). DAPI can be used to stain eukaryotic nuclei and is mainly used in fixed cells, as it is toxic to live cells. DAPI can stain bacteria more faintly than mammalian cells (Biotium, 2022). Cappello et al. (2011) used DAPI to enumerate bacterial abundance in the gills of mussel *Mytilus galloprovincialis* in a contaminated environment. Here, I use DAPI to visualize both symbionts and host nuclei in *Thyasira* cf. *gouldi* gill cells.

1.3.4 Phalloidin

Phalloidin is a toxin isolated from the *Amanita phalloides* “death cap” mushroom that can be used to label cellular structures made of F-actin. Here, I use Alexa Fluor 488 phalloidin from

ThermoFisher Scientific which is the phalloidin probe conjugated to the green-fluorescent dye. In a comparison of multiple conjugated phalloidin probes, Alexa Fluor 488 phalloidin was ranked as the best (DesMarais et al., 2019). I use phalloidin to visualize the cell membrane, endocytotic and cytoskeletal structures of the bacteriocytes in *Thyasira* cf. *gouldi* gill filaments.

1.3.5 LysoTracker

LysoTracker Deep Red (ThermoFisher Scientific) is a cell-permeable fluorescent stain that targets acidic organelles in live cells. LysoTracker has been developed for cultured mammalian cells, but has been used in molluscs: Mateo et al. (2009) used flow cytometry along with LysoTracker to characterise the change in haemocytes in a soft-shelled clam when introduced to two strains of *Vibrio splendidus*, and Tame et al. (2022) used the same stain to document lysosomal digestion of endocytosed bacteria in epithelial cells of the gills of the deep-sea mussel *Bathymodiolus japonicus*. Here I use LysoTracker Deep Red to visualize potential lysosomes and other structures which could indicate digestion of symbionts in *Thyasira* cf. *gouldi* gill filaments.

1.4 Objectives

This thesis focuses on the development of new approaches to visualize symbionts and host cellular features in whole mounts of thyasirid gills using fluorescence labelling and high-resolution confocal microscopy. Combinations of fluorescent stains (up to three per preparation) and various staining procedures were used on dissected gills to assess repeatability and consistency of approaches. The fluorescent stains were selected considering emission wavelengths to reduce likelihood of co-localization; some stains could not be used with others emitting at a similar wavelength (e.g. CTC and LysoTracker DeepRed). The use of phalloidin

conjugated with green Alexa 488 fluor dye enabled combined use with DAPI (blue) and CTC/LysoTracker (red).

For some gills, a fragment was prepared for transmission electron microscopy to compare features using both approaches. In addition, a review of a collection of previously obtained transmission electron micrographs of *Thyasira* cf. *gouldi* gills was performed to characterize intracellular structures (membrane whorls, lysosomes, phagolysosomes, residual bodies) that could represent distinct stages of symbiont digestion. Micrographs included those generated in a study that characterized temporal patterns in symbiont abundance in *Thyasira* cf. *gouldi* from Bonne Bay sampled at different months (Laurich et al., 2015) as well as in a study of specimens maintained in thiosulfate-enriched conditions (Laurich et al., 2018). Other gills prepared by J. Laurich for an unpublished study of "starved" specimens kept in seawater without particulate food, sediment or reduced sulfur were examined. All gills were prepared as described in Laurich et al. (2015).

In this thesis, different combinations of selected fluorescent stains are tested, along with their ability to reveal structures of interest in *Thyasira* cf. *gouldi* gills. Specifically, symbiont labelling was performed using CTC, Propidium Iodide and DAPI, while host actin was labeled with phalloidin, host nuclei were labeled using DAPI, and lysosomes were labeled using LysoTracker.

Chapter 2: Materials and Methods

2.1 Study site

Specimens of *Thyasira* cf. *gouldi* were collected from the Bonne Bay fjord, Newfoundland and Labrador, Canada. Collection sites included Deer Arm (N 49º33.150-190; W 57º50.400-520) and Southeast Arm (N 49º27.740-760; W 57º43.320-400 and N 49º27.800; W 57º42.855) at ~30 m depth (Fig. 3).

2.2 Sample Collection

Sediments were collected from multiple grab samples on May 24, 2022 from Deer Arm and Southeast Arm using a Peterson grab and a mechanical haul. The sediments obtained from the grab were placed in labeled bins to take back to the field station. At the field station, the sediment was sieved through a 1-mm mesh sieve, with sediment having passed through the sieve being retained for later use. Material remaining on the sieve was rinsed with running seawater, and all visible bivalves were carefully collected using entomological forceps. Bivalves were then sorted into thyasirids and "others". The thyasirids, which measured in size between 3-5mm, were placed in a jar with chilled seawater and transported on ice back to the St. John's campus for further sorting.

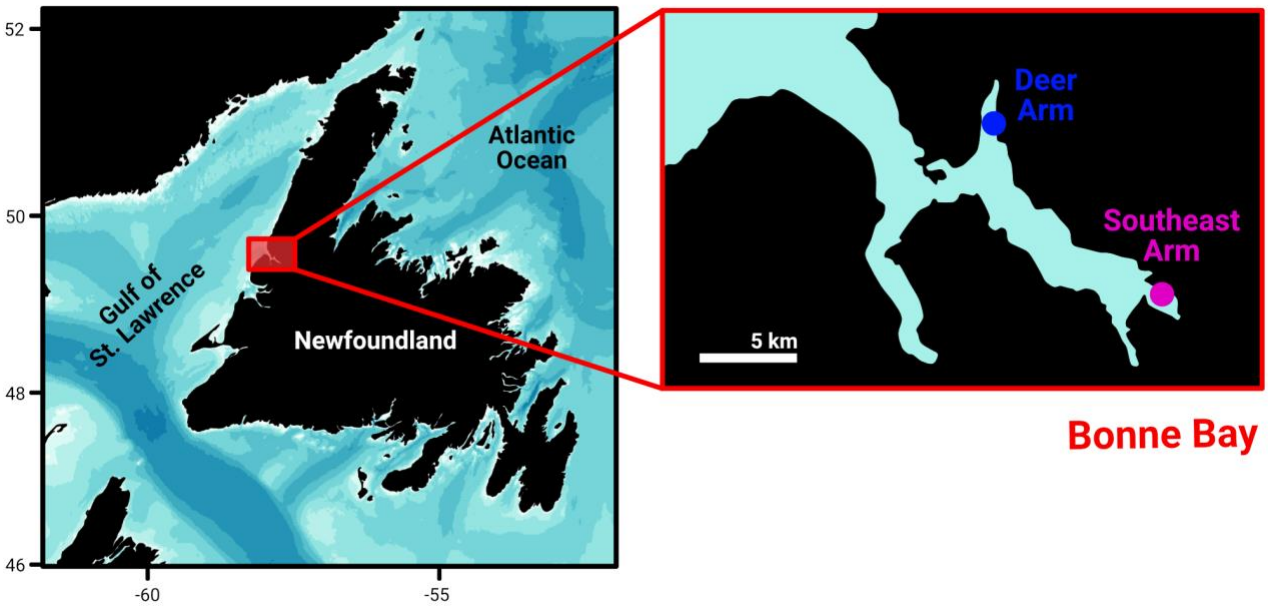

Figure 3. Maps of sites sampled in Bonne Bay, NL. Produced by Valentin Kokarev.

2.3 Specimen Maintenance

Upon arrival, thyasirids were sorted into "symbiotic" *T*. cf. *gouldi*, "asymbiotic" *T*. cf. *gouldi* (OTU 3), and "*Parathyasira*" (an asymbiotic taxon of thyasirids) using a stereoscope based on shell shape (Batstone et al., 2014). A large Rubbermaid container (61 cm x 40.6 cm x 31.8 cm) was filled halfway with seawater obtained from the Ocean Sciences Centre at Logy Bay, Newfoundland and Labrador, and placed in a cold room set at 4ºC with an airstone attached to provide aeration. Thirteen mini aquaria (10.5 cm x 5.5 cm x 10.5 cm) were filled to about ¾ capacity with sieved sediment, with one labeled "others", one labeled "asymbiotic", five labeled "*Parathyasira*", and six labeled "symbiotic". The labels were made using a toothpick and different coloured tape representing each type – green (asymbiotic), orange (*Parathyasira*), red (symbiotic), and white (others). Each mini aquarium contained ~6-10 clams to be kept alive for a period of 6 months, and specimens were retrieved as needed to perform fresh dissections and gill preparations (Fig. 4). Staining preparations began ~2 weeks after collection and the last specimens were processed 6 months after being placed in aquaria (Appendix A).

2.4 Sample Preparation

Prior to staining, thyasirids (asymbiotic or symbiotic) were obtained by scooping some sediment out of a mini aquarium onto a 1 mm mesh sieve in the lab and rinsing using seawater. The bivalves were then put into a petri dish with some seawater to be dissected. Asymbiotic specimens were used solely to practice dissections and initial staining procedures and will not be further discussed.

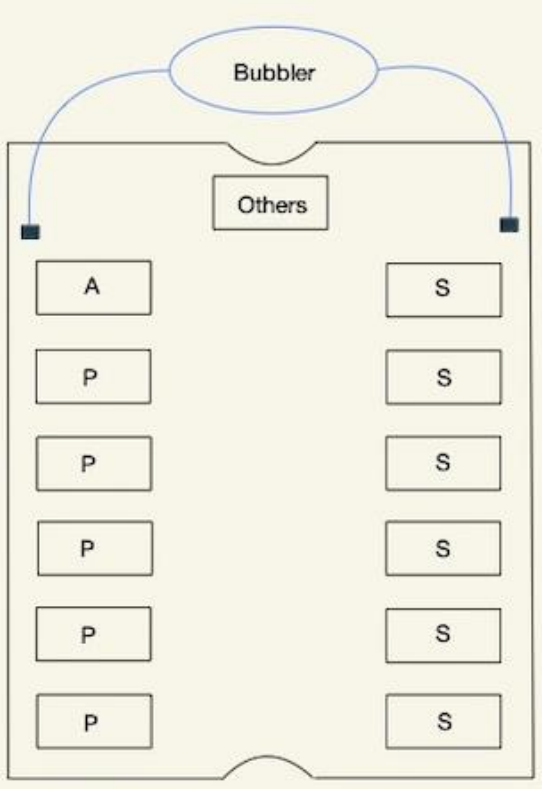

Figure 4. Schematic of the Rubbermaid bin containing mini aquaria filled with sediment for specimen maintenance in the cold room (4°C), as viewed from above. Schematic generated using Notability.

2.5 Dissection and Gill Extraction

A small piece of Parafilm was placed on the stage of a stereoscope along with the bivalve. The shell was measured from the hinge to the ventral margin, then dissected by wedging the thyasirid under a gloved finger and slipping a scalpel between the shells to sever the adductor muscles. The shells were then pried apart, exposing the internal organs. A drop of saltwater was then placed on each shell to float the pallial organs. Using a pair of fine forceps, the gills were removed and placed onto individual slides for staining. In some cases, the gills were divided into two halves (anterior and posterior) using a scalpel. Both halves were either processed in the same way, using the different combination of stains or with one half examined with TEM whereas the other half was viewed with the confocal microscope. All available specimens (total of 20) were dissected and stained with various dyes and/or prepared for TEM (Appendix A).

2.6 Fixation and permeabilization for confocal microscopy

Before using stains that are toxic or impermeable to live cells (such as phalloidin, PI, and DAPI), the gills were fixed using 25 µL 4% formaldehyde for 15 minutes then rinsed with Phosphate Buffered Saline (PBS) for 5 minutes. To permeabilize the cells, 25 µL of 0.1% Triton X-100 in PBS was applied onto the gill for an additional 15 minutes, then rinsed with PBS for 5 minutes.

2.7 Staining for confocal microscopy

Staining was done using different combinations to avoid overlap in emission wavelengths. Phalloidin and DAPI worked excellently together as they are green and blue, respectively. However, CTC and LysoTracker DeepRed could not be used together as they are both shades of red and it would be impossible to differentiate them due to the emission spectra. Phalloidin and DAPI could be used with either CTC or LysoTracker, but not both (Fig. 5).

2.7.1 CTC (5-cyano-2,3-ditolyl tetrazolium chloride)

To make a stock solution from the 5-cyano-2,3-di(p-tolyl) tetrazolium chloride powder (Sigma-Aldrich, 2023), 5 mg was dissolved in 0.33 ml of distilled water and put in the freezer. Upon use, 1 µL of CTC was placed in 100 µL of PBS with 50 µL used per gill. The gill with CTC was then left to incubate in 4°C for 2-4 hours in the dark. After incubation, the gill was then rinsed 3 to 5 times with PBS before fixing and other staining (CTC was used in combination with phalloidin and DAPI).

2.7.2 LysoTracker

The 1 mM probe stock solution of LysoTracker Deep Red (ThermoFisher Scientific) was diluted in PBS (0.5 µL in 10 mL) to a working solution of 50 nM. Since this is a live stain, 25 µL of the working solution was pipetted onto the gill immediately after dissection and left to incubate in the dark at 4°C for 2 hours, as per the protocol followed in Mateo et al. (2009). After the incubation period, the staining solution was removed by pipetting and replaced with ~50 µL of PBS, repeated three times. The gill was then fixed and permeabilized for further staining with phalloidin and DAPI.

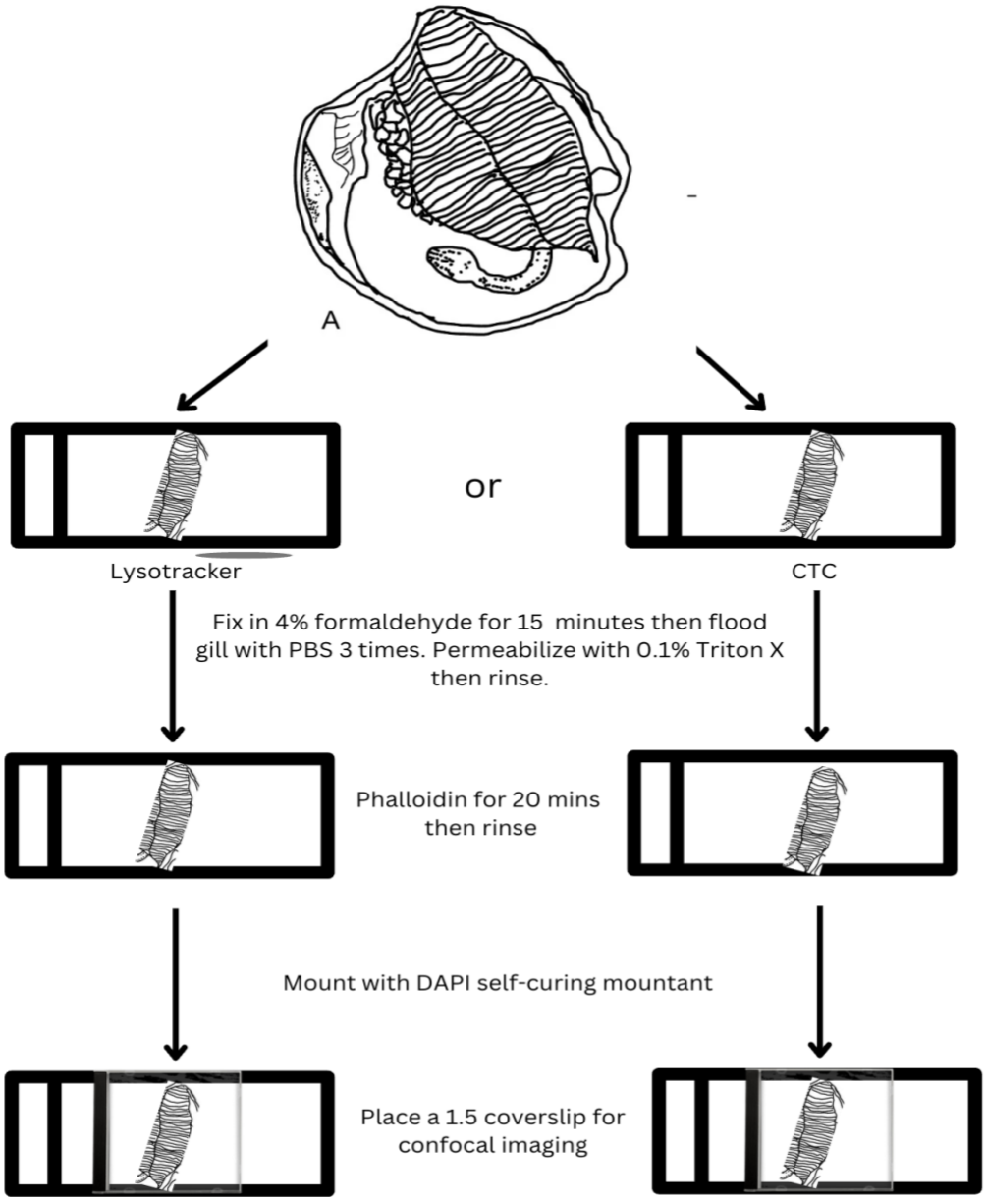

Figure 5. Flow chart representing staining procedure for confocal microscopy. Flow chart created using Canva.

2.7.3 Propidium Iodide

After fixing and permeabilization, 25 ml of PI 1mg/ml solution in distilled water (Molecular Probes Inc.) was pipetted onto the gill and left in the dark for 5 minutes. The PI was removed by pipetting and replaced with ~50 µl of PBS and repeated three times. The gill was then fixed and permeabilized for further staining with phalloidin and DAPI.

2.7.4 Phalloidin

Prior to mounting, the gill was stained with Alexa Fluor 488 phalloidin. As per ThermoFisher Scientific protocol, a 400X stock solution was made by dissolving the vial contents in 150 µL of anhydrous DMSO then aliquoted into Eppendorf tubes containing 5 µM stock solution and stored at -20°C. Upon use, the aliquots were thawed and 0.5 µl was added to 200 µl PBS for a working solution. As the last stain before mounting, the gill was flooded with ~25 µL phalloidin and incubated for 20 to 25 minutes in the dark at room temperature in a drawer with PBS at the bottom to maintain a humid environment. After incubating, the phalloidin was then pipetted off followed by the gill being flooded with PBS (and removed) three times. The gill was then ready to be mounted.

2.7.5 DAPI staining and mounting

After the staining process was done, ~25-40 µL of ProLong Gold antifade reagent with DAPI (Thermo Fisher Scientific) was pipetted onto the sample and covered with a 1.5

microscope cover glass (Globe Scientific Inc.). The mounted slides were left at 4˚C overnight for curing prior to microscopy and imaging.

2.8 Confocal Laser Microscopy

The slides with the stained gills were observed using a confocal laser microscope (Zeiss LSM 900 with Airyscan 2) at the Electron Microscopy Unit in the Faculty of Medicine, Memorial University of Newfoundland. Each stain was viewed using the appropriate filter for each excitation and emission wavelength (Table 1). Airyscan 2 is an area detector using 32 circularly arranged element detectors that individually act as a pinhole to create a super high-resolution image (Zeiss, 2023). Some images were taken using Airyscan 2 mode as it provides higher resolution images for smaller structures such as bacteria and nuclei. Images were captured based on clarity of structures and areas where staining quality was highest. Scale bars were added using Zeiss ZEN Microscopy Software and images exported as TIFF files.

Table 1: Stains used along with their excitation/emission wavelengths, the confocal filter set used, and targeted structures.

Stain used	Excitation/Emission (nm)	Filter used	Structure targeted
Alexa Fluor 488 Phalloidin	495/518	Alexa 488	F-actin
DAPI	358/461	DAPI	Host nuclei
			Symbionts
LysoTracker DeepRed	647/668	Cy5	Acidic organelles
CTC	450/630	Alexa 610	Respiring symbionts
Propidium Iodide	535/617	Alexa 610	Inactive bacteria

2.9 Processing for Transmission Electron Microscopy

Gills were cut into 2 pieces, and half-gills were processed for TEM and confocal microscopy (Fig. 6). For TEM, half-gills were fixed in 2.5% glutaraldehyde at 4°C then transferred to PBS. After fixing, the gills were immersed in 1% osmium tetroxide (OsO_4) in PBS for 15 minutes. The gills were then dehydrated in 50%, 70%, 90%, and 100% (twice) ethanol for 15 minutes and then embedded in EPON resin. The resin blocks were then left to cure overnight in the embedding oven at 80°C.

Embedded gills were sectioned on a Leica Reichert Ultracut S ultramicrotome, and ultrathin sections placed onto copper grids. Sections were poststained with UranyLess Contrast Stain Solution (Electron Microscopy Sciences) and lead citrate prior to imaging on Tecnai G^2 Spirit 120 kV transmission electron microscope at the Electron Microscopy Unit in the Faculty of Medicine, Memorial University of Newfoundland.

2.10 Examination of previously obtained TEM images

Membrane whorls and potential lysosomal bodies, phagolysosomes and residual bodies were examined in a collection of published and unpublished TEM images (N = 471) of *Thyasira* cf. *gouldi* gills available in the Dufour laboratory at Memorial University of Newfoundland. These micrographs included gills of specimens that had been collected at different times of the year, when symbiont abundance differed (Laurich et al., 2015) and experimental subjects that had been maintained in sodium thiosulfate (Laurich et al., 2018). In addition, the collection included micrographs of specimens from an unpublished study by J. Laurich of *T.* cf. *gouldi* specimens that were “starved”, i.e. maintained in containers of chilled, filtered seawater, with no added particulate food or sediments, for a period of 40 days, and then transferred to containers of

native sediment for 16 days (specimen were dissected and fixed at different times during this period). The main goals of the latter experiment were to test whether symbiont abundance would decrease over the 40 days, and whether symbionts would be re-acquired after replacing in sediments. Specimens that had been maintained with constant exposure to thiosulfate or in a starvation state could be expected to show divergent intracellular features as a response to different environmental conditions.

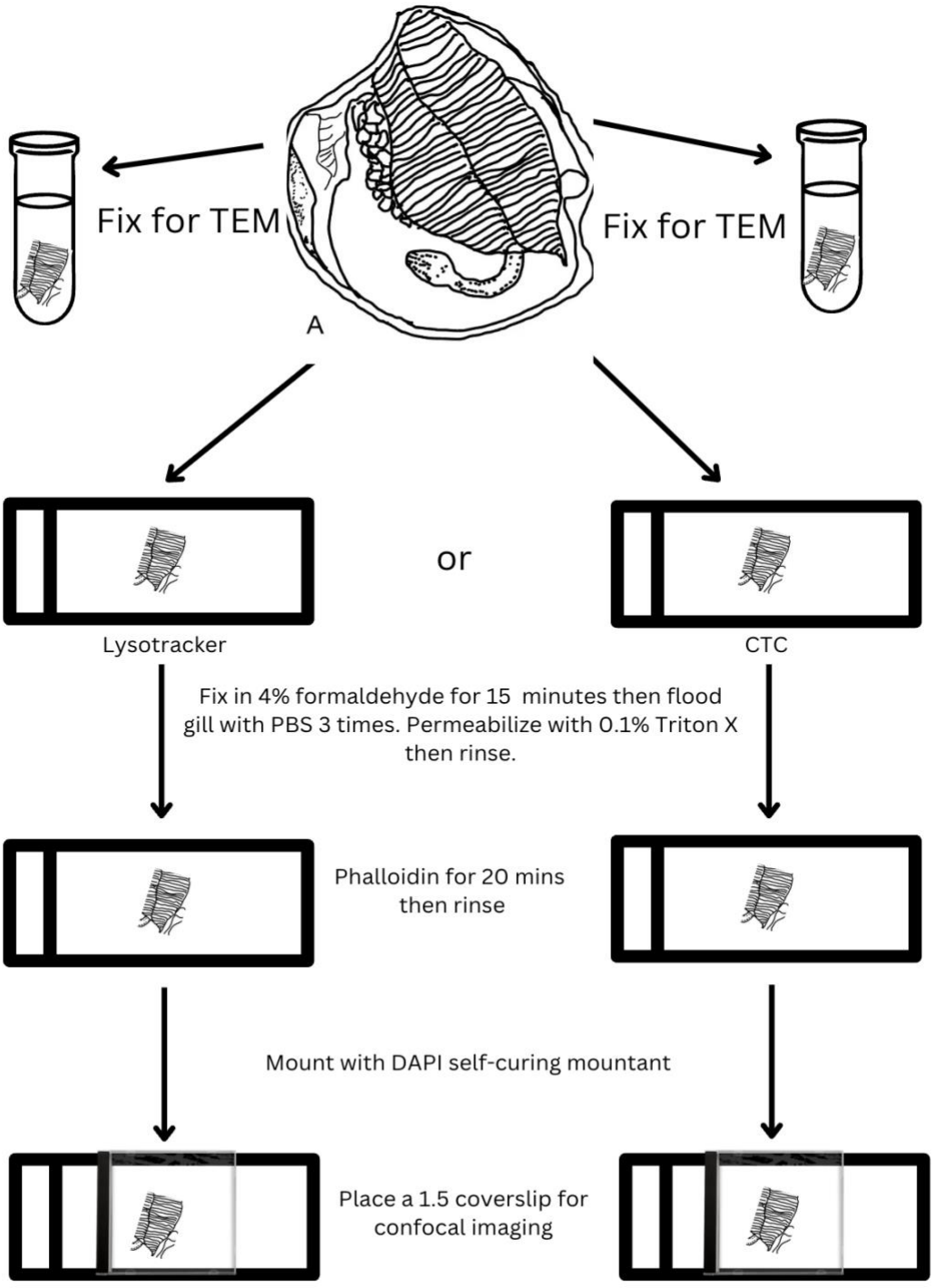

Figure 6: Flow chart showing the prep for TEM and the matching confocal gills. Flow chart created using Canva.

Chapter 3: Results

I observed whole-mounts of entire half-gills processed using various combinations of stains with confocal microscopy in attempts to visualize bacteriocyte structures (host cell membranes, host nuclei, phagocytotic or lysosomal structures) as well as symbionts. I aimed to identify procedures yielding results that were repeatable across replicates of gills from the same, or different *Thyasira* cf. *gouldi* individuals. The preparation of Z-stacks following imaging of consecutive optical sections provided novel views of bacteriocytes and other gill structures. These new perspectives of bacteriocytes were compared with TEM images from the same specimens.

This work was complemented with a review of a library of TEM images obtained from previous observational and experimental work done on *Thyasira* cf. *gouldi*. I present a compilation of micrographs on which I characterize features of membrane whorls along with their relationship with bacterial symbionts, some of which appear to be undergoing digestion.

3.1 Labelling of host cell structures

The stains and procedures used collectively allowed visualization of host nuclei (DAPI; Figs. 7-10), the margins of epithelial cells (phalloidin; Figs. 7, 9) and possible acidic organelles (LysoTracker; Fig. 8).

3.1.1 Phalloidin

I used phalloidin to label filamentous actin in *Thyasira* cf. *gouldi* gill bacteriocytes, with the intention of observing cell membranes as well as the phagocytosis of bacterial symbionts.

Phalloidin labeled actin in almost every trial (12 out of 13 times) with a 92.31% success rate. Phalloidin effectively stained the membranes of gill cells that were in contact with the external medium (Fig. 7B), which facilitated interpretation of tissue and cell orientation. The two layers of epithelial cells on either side of the hemolymph (gill blood space) could be readily seen on gill filaments, with phalloidin labelling appearing as a row of bright green structures at the distalmost margin of epithelial cells, corresponding to the tips of microvilli (Fig. 7B-D). In some cases, phalloidin labeled membranes between adjacent epithelial cells (Fig 7C). When phalloidin was used in combination with CTC, both appeared to colocalize on the same structures (Fig. 9C) at the distal boundary of cells. Although phalloidin was expected to label phagocytotic structures, which would be engulfing bacteria at the proximal end of cells, no such labelling was observed. With phalloidin staining, the locations where symbionts are expected to be found in the gill cells could be situated as being between host nuclei and the outermost microvillar cell layer (Fig. 7C).

3.1.2 DAPI

I used DAPI, which stains nucleic acids, to visualize host nuclei along with bacterial symbionts. DAPI had a 92.31% success rate when labelling host nuclei (Fig. 7A). On a few occasions, cilia or cirri were stained by DAPI (Fig. 8D). However, I did not see any labelling of bacterial symbionts using DAPI.

Table 2. Fluorescent staining details and apparent labelling rates using confocal laser microscopy

Stain used	**Targeted structure**	**Total times used**	**Times intended structures labeled**	**% success**
DAPI	Host nuclei	28	27	92.31
CTC	Respiring bacteria	13	6	46.15
Phalloidin	F-actin	13	12	92.31
LysoTracker	Acidic organelles	7	3	42.86
Propidium Iodide	Inactive bacteria	3	0	0

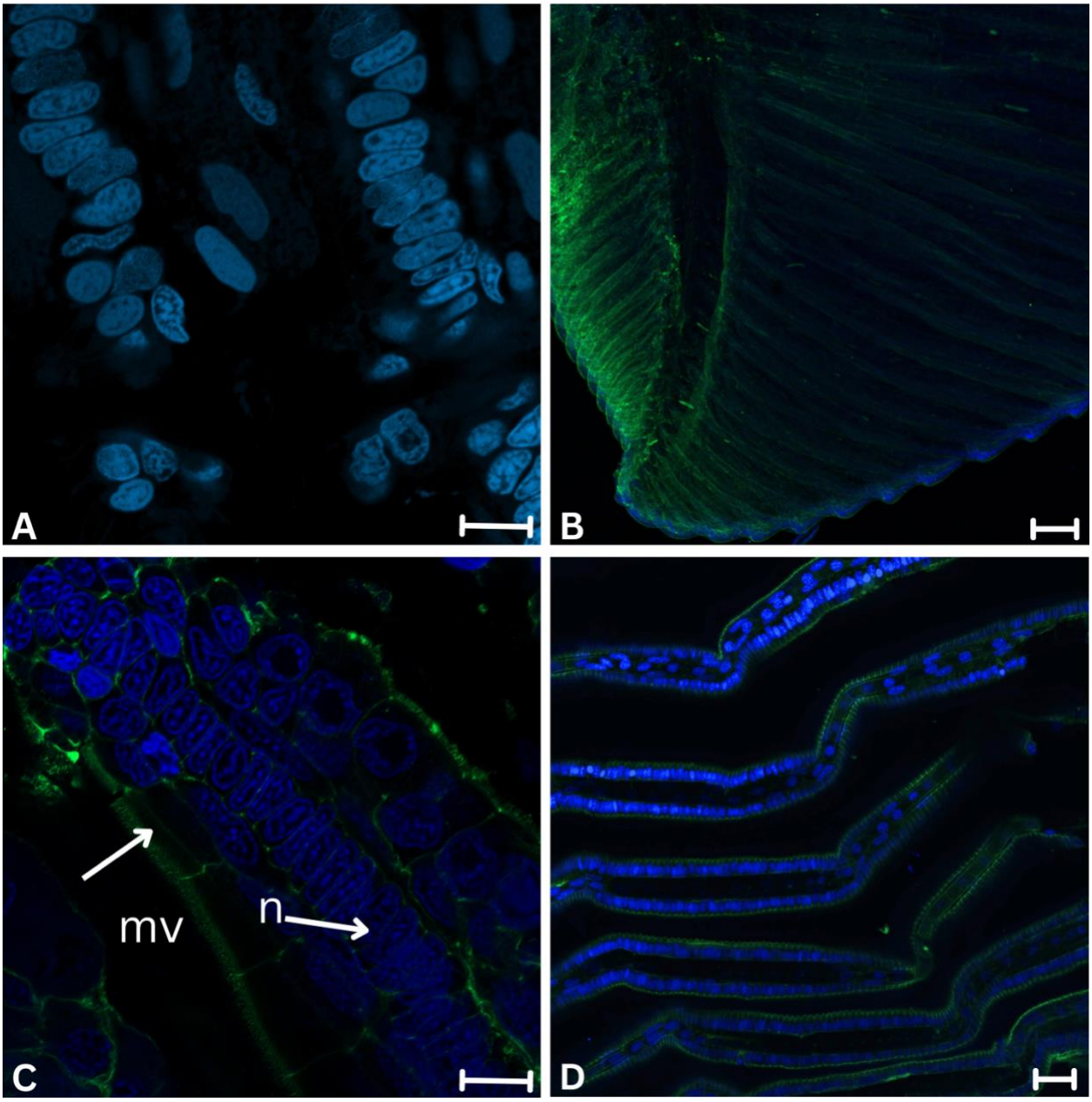
A
B
C
mv
n
D

Figure 7. Whole mounts of *Thyasira* cf. *gouldi* gills labeled stained with DAPI only (A), or with both DAPI and Phalloidin (B-D), viewed using Zeiss LSM 900 confocal microscopy. Scale bars: A, C = 10 μm, B = 100 μm, D = 20 μm. **A)** Gill cells stained with DAPI only, revealing host nuclei but no symbionts, imaged under Airyscan mode at 63X. **B)** Phalloidin staining revealing the outline of gill filaments (green), with some DAPI staining visible at the ventral extremity of filaments (blue), under confocal mode, 5X. **C)** Gill filaments viewed with Airyscan mode at 63X, with distal ends of epithelial cells and membranes between adjacent cells labeled with phalloidin (green), while host nuclei are stained with DAPI (blue). The arrow indicates where the symbionts were expected. **D)** Rows of gill filaments revealing phalloidin staining of distal ends of cells (green), with host nuclei at the proximal end of the same cells stained with DAPI (blue) under confocal mode at 20X. Labels: mv: microvilli; n: nuclei.

3.1.3 LysoTracker

I used LysoTracker with the intent of labelling lysosomal activity in the bacteriocytes. Of the 7 times we used LysoTracker, it only labeled potential acidic organelles – assumed to be lysosomes – three times, yielding a success rate of 42.86% for labelling acidic organelles in *Thyasira* cf. *gouldi* gills. In gills that showed positive LysoTracker labelling, only a few labeled structures were seen after searching through entire gill fragments. The LysoTracker labeled other structures inside and outside cells twice which we did not expect to be acidic, such as cilia and cirri, the double rootlets of which are visible as distinct rows in Fig. 8A. More expected, specific labelling of what appears to be acidic organelles (suspected lysosomes) in the cell is seen in Fig. 8B.

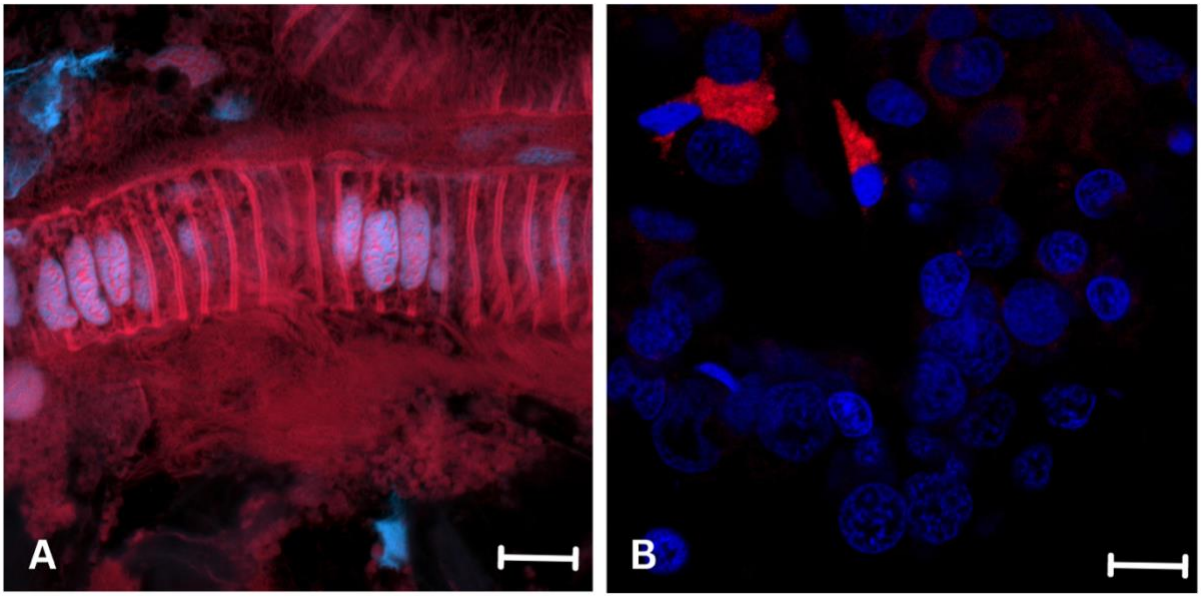

Figure 8. Whole mounts of *Thyasira* cf. *gouldi* gills viewed using Zeiss LSM 900 confocal microscopy with Airyscan mode following labelling with LysoTracker and DAPI. Scale bars = 10 µm. **A)** DAPI labelling host nuclei (blue) along with LysoTracker (red) labelling laterofrontal cirri, appearing as distinct rows where fused at their proximal end. **B)** DAPI labelling host nuclei (blue) along with LysoTracker (red) labelling potential lysosomes (acidic organelles).

3.2 Labelling of symbionts

3.2.1 CTC (5-cyano-2,3-ditolyl tetrazolium chloride)

I used CTC to visualize active symbionts via respiratory activity. When the symbionts undergo respiration, a red-fluorescing precipitate (CTC-formazan) is produced in the cell when it is reduced by the electron transport system of the bacteria (Créach et al., 2002). Of the thirteen times CTC was used, bacterial symbionts were only visible six times (46% expected labelling success).

Using phalloidin together with CTC yielded expected results in some cases (Fig. 9A,B), but in other instances there appeared to be colocalizing of CTC and phalloidin, which provided less useful cues on cell orientation, and no evident bacterial labelling (Fig. 9C). As this happened multiple times, I performed subsequent staining procedures without phalloidin, using only DAPI and CTC (Fig. 9D-F). The combination of DAPI and CTC revealed potential respiring bacterial symbionts (~5 µm) labeled in red, but due to the lack of phalloidin, the location of these structures in gill filaments could not be ascertained.

In one gill, I observed an enlarged structure appearing to be a nodule containing *Rickettsia*-like bacteria labeled by CTC (Fig. 9A, B). *Rickettsia*-like organisms (RLO) are intracytoplasmic in numerous bivalve and mollusc tissues, found in vacuolar inclusions (Cruz-Flores et al., 2020).

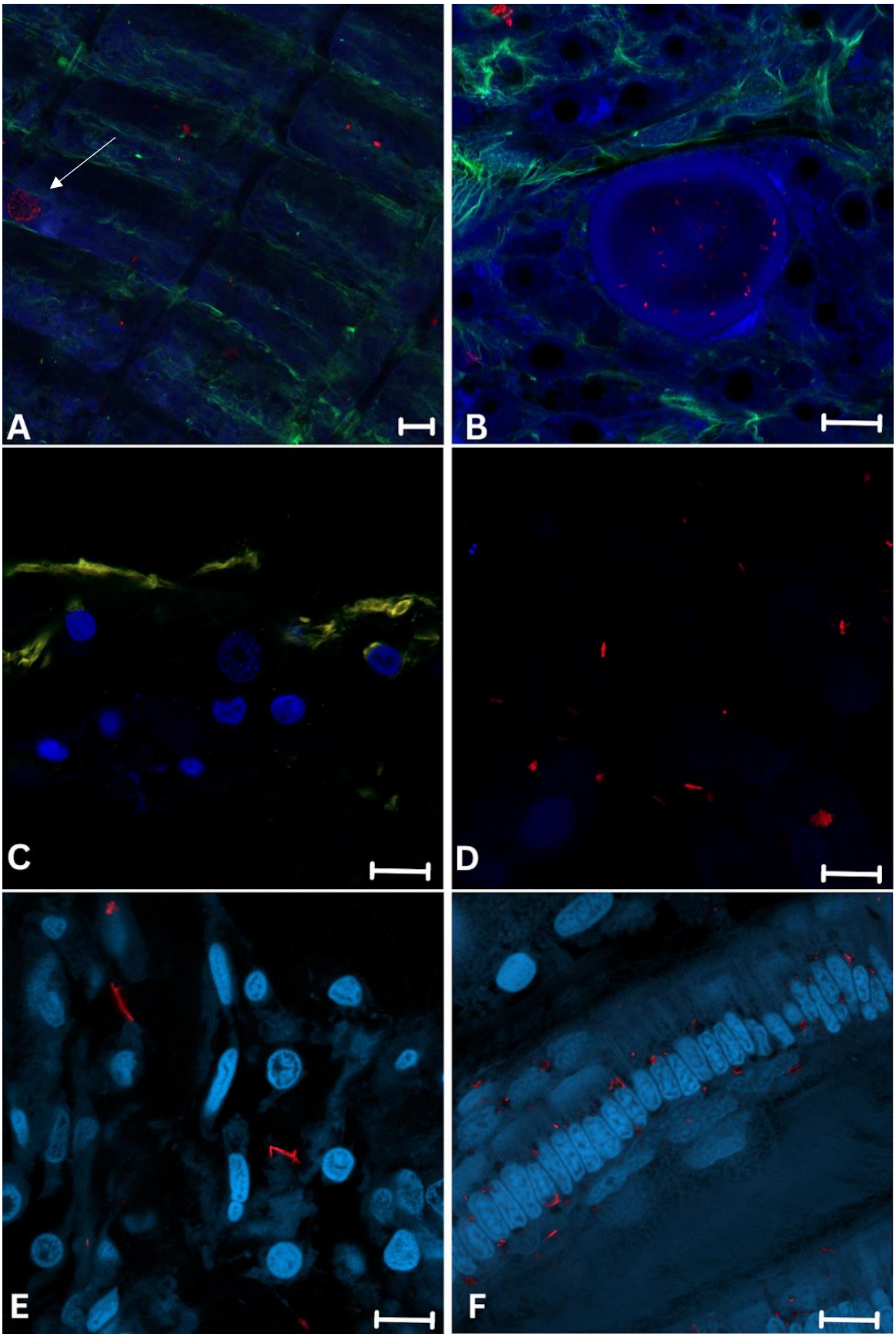
A
B
C
D
E
F

Figure 9. Whole mounts of *Thyasira* cf. *gouldi* gills viewed using Zeiss LSM 900 confocal microscopy and with Airyscan mode. Scale bars: A = 20 μm; B, C, D, E, F = 10 μm. **A)** Phalloidin labelling F-actin (green), DAPI labelling nuclei (blue) and CTC labelling potential symbionts and other bacteria (red) with arrow pointing at a *Rickettsia*-like nodule in the gill filament at 20X, **B)** The *Rickettsia*-like nodule viewed at Airyscan 63X with phalloidin labelling F-actin (green), DAPI labelling nuclei (blue) and CTC labelling potential symbionts and other bacteria (red). **C)** Combined Phalloidin, CTC, and DAPI staining. Host nuclei are visible in blue (DAPI). Yellow colouration may be related to a reaction of phalloidin with CTC, potentially labelling actin. **D)** DAPI staining the nuclei and CTC potentially labelling respiring symbionts. **E)** and **F)** DAPI labelling nuclei (blue) and CTC labelling potential symbionts (red) imaged using Airyscan mode at 63X.

3.2.2. Propidium Iodide

I used the live/dead stain PI in an attempt to label dead/dormant symbiotic bacteria in *Thyasira* cf. *gouldi* gill bacteriocytes. I used PI three times and only observed very faint (inconclusive) labelling of potential bacterial symbionts. However, it did label host nuclei all three times it was used (Fig. 10C, D), making it 100% accurate for nuclear labelling. Aligned nuclei (pink) are visible in the gill filaments cells (Fig. 10B) outlined by phalloidin (green). The nuclei appear pink instead of red due to colocalizing of DAPI and PI, both staining the nuclei. In the ciliated zone of filaments, cilia or cirri were stained blue by DAPI (Fig. 10D). Imaging in non-ciliated regions uncovered only very faint staining by PI between the nuclei and microvillar border (Fig. 10C), suggesting the presence of some dead symbionts in *Thyasira* cf. *gouldi.*

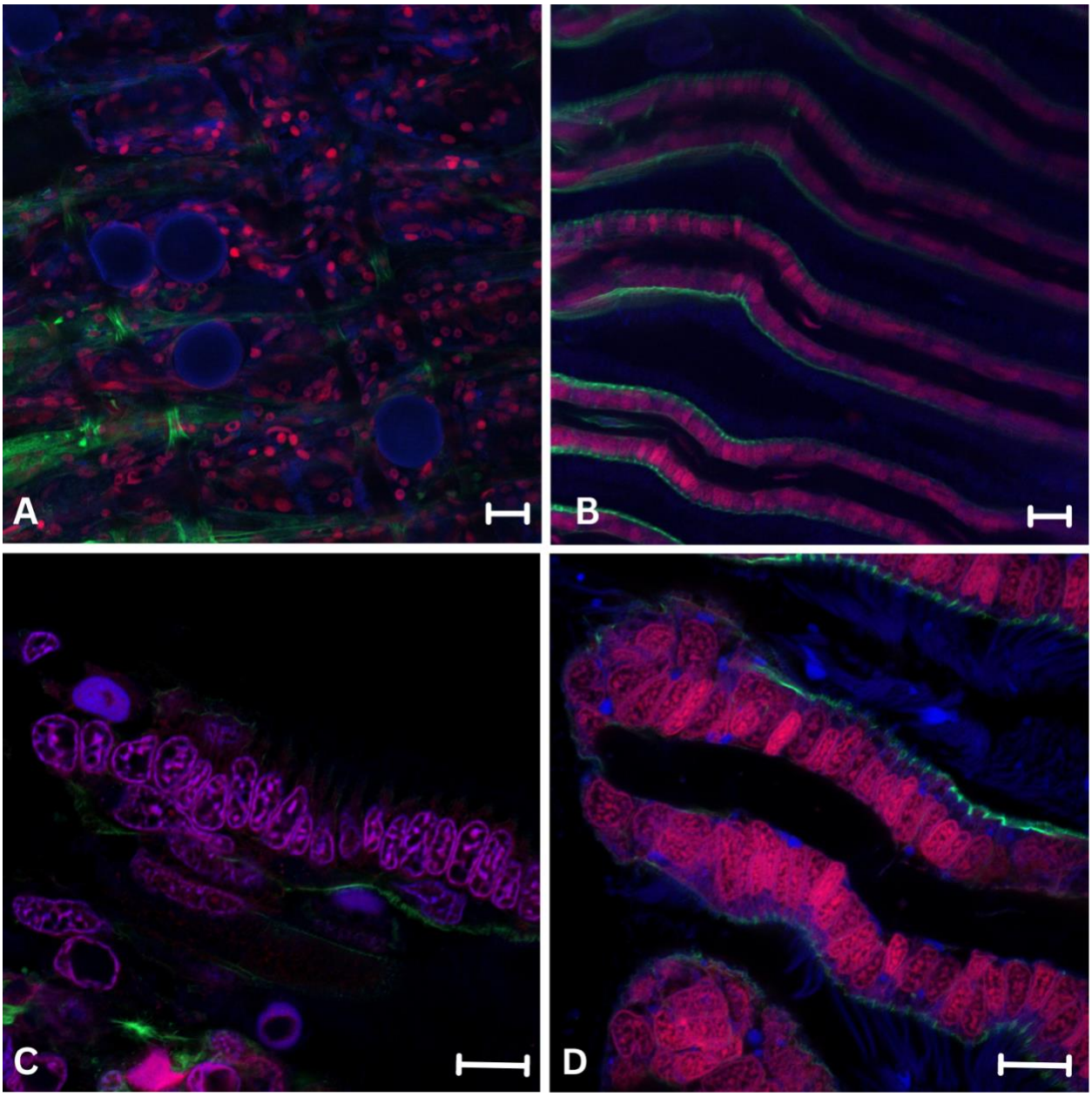
A
B
C
D

Figure 10. Whole mounts of *Thyasira* cf. *gouldi* gills stained with Propidium iodide (PI, red), phalloidin (green) and DAPI (blue), viewed using Zeiss LSM 900 confocal microscopy. Scale bars: A, B = 20 µm, C, D = 10 µm. **A)** PI and DAPI co-labelling host nuclei (pink), phalloidin (green) labelling cytoskeleton, and DAPI (blue) labelling the outside of large, spherical objects suspected to be kidney concretions. **B)** Phalloidin (green) labelling cytoskeletal structures, PI and DAPI co-localizing to host nuclei (pink). **C)** Airyscan image taken in bacteriocyte zone, with some possible dead symbionts faintly stained by PI between nuclei and the tips of microvilli. **D)** Airyscan image from the ciliated zone of filaments, with phalloidin labelling tips of microvilli, propidium iodide and DAPI co-localizing to host nuclei, and cilia or cirri labeled by DAPI.

3.3 Transmission Electron Microscopy of corresponding half-gills

Half-gills prepared for TEM in the present study revealed rod-shaped symbionts in the specimens examined, as well as some membrane whorls (Fig. 11). Many symbionts contained apparently empty vesicles, likely elemental sulfur granules that dissolved during processing (Vetter & Fry, 1998). The bacterial abundance and the extracellular space occupied by symbionts were relatively low, as expected in thyasirids sampled in the spring (Laurich et al., 2015). In addition, the prolonged (5 month) aquarium maintenance, even within native sediments and in temperatures representative of those experienced in their environment, could have resulted in a decrease in symbiont abundance.

Notably, symbiont abundance in a half-gill examined by TEM (Fig. 11) appeared greater than in the other half, stained with CTC and DAPI. It is likely that the CTC did not label all symbionts present, which could indicate that only a fraction of the symbionts was actively respiring at the time of processing.

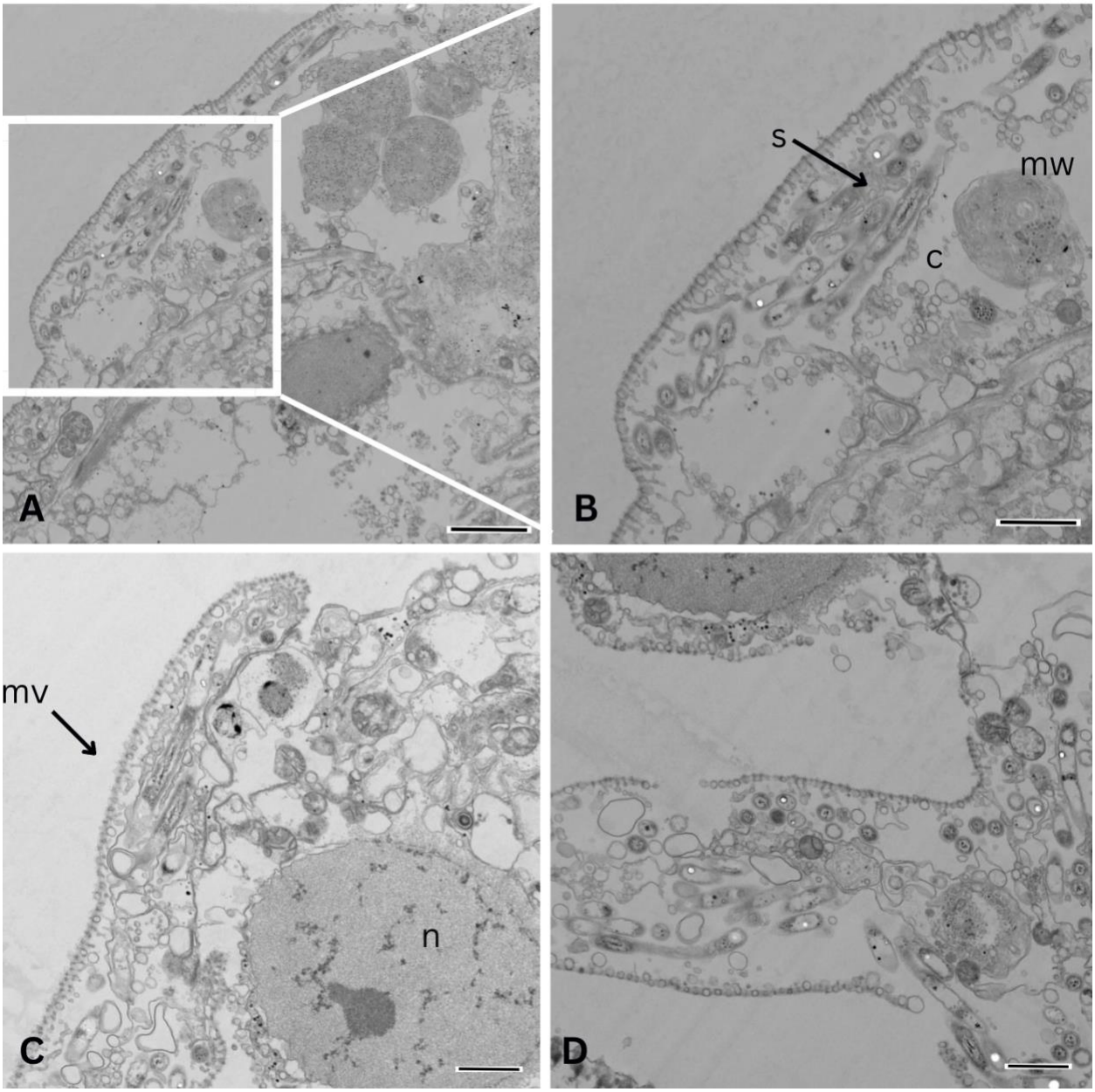
A
B
s
mw
c
C
mv
n
D

Figure 11. TEM micrographs of bacteriocytes of *Thyasira* cf. *gouldi* from the present study, collected in May 2022 and fixed in October 2022. Half of the same gill was processed for confocal microscopy. **A)** and inset **B)** show symbionts (s) visible in the extracellular space, bordered by microvilli (mv) and the bacteriocyte cell membrane. Membrane whorls (mw) are visible in bacteriocyte cytoplasm (c). **C)** and **D)** show other bacteriocytes from the same specimen, with symbionts visible in a thin extracellular layer, bounded by microvilli. Scale bars: A = 2 μm; B - D = 1 μm. n: nucleus.

3.4 Observations of membrane whorl features on previously prepared TEM images

In ultrathin sections of bacteriocytes, membrane whorls appear in a range of sizes, with the density, quantity and distinctiveness of whorls varying across and within cells (Fig. 12A-D). In some instances, membranes were loosely packed and distinct rings could clearly be seen, with little to no material visible within the structure (**asterisk**, Fig. 12B). Some irregularly shaped lysosomes included more electron-dense, tightly packed membranes with multiple inward folds (**ly** in Fig. 12A, D). Several examples of distinct membrane whorls that were in close contact with each other, or even clusters of smaller whorls enveloped by a larger membrane, were observed (**arrowheads**, Fig. 12B-D). Some (particularly larger sized) membrane whorls or clusters of membrane whorls seemed to have a high number and density of membranes, giving the structure an almost uniform, electron-dense (dark grey) aspect (**mw**, Fig 12A).

Membrane whorls were dispersed throughout the cytoplasm of bacteriocytes from the basal to the apical ends, and appeared to occupy more cytoplasmic space overall than the nucleus on the ultrathin sections observed (e.g. Fig. 13A). Within some membrane whorls, one or more bacterial symbionts were visible (Fig. 13B-F; 14A-D). The symbionts often seemed be located within the centre of a whorl, including in instances where clusters of adjoining whorls were visible (Fig. 13B), but this was not always evident (Fig. 13D). Symbionts within whorls were generally distinguishable from groups of symbionts seemingly surrounded by host membrane in what might be vesicles lacking any apparent whorls (**asterisk** on Fig. 12C, **arrowhead** on Fig. 13C). In some instances, bacteria visible within whorls appeared to be degraded (**asterisk** in Fig. 14A).

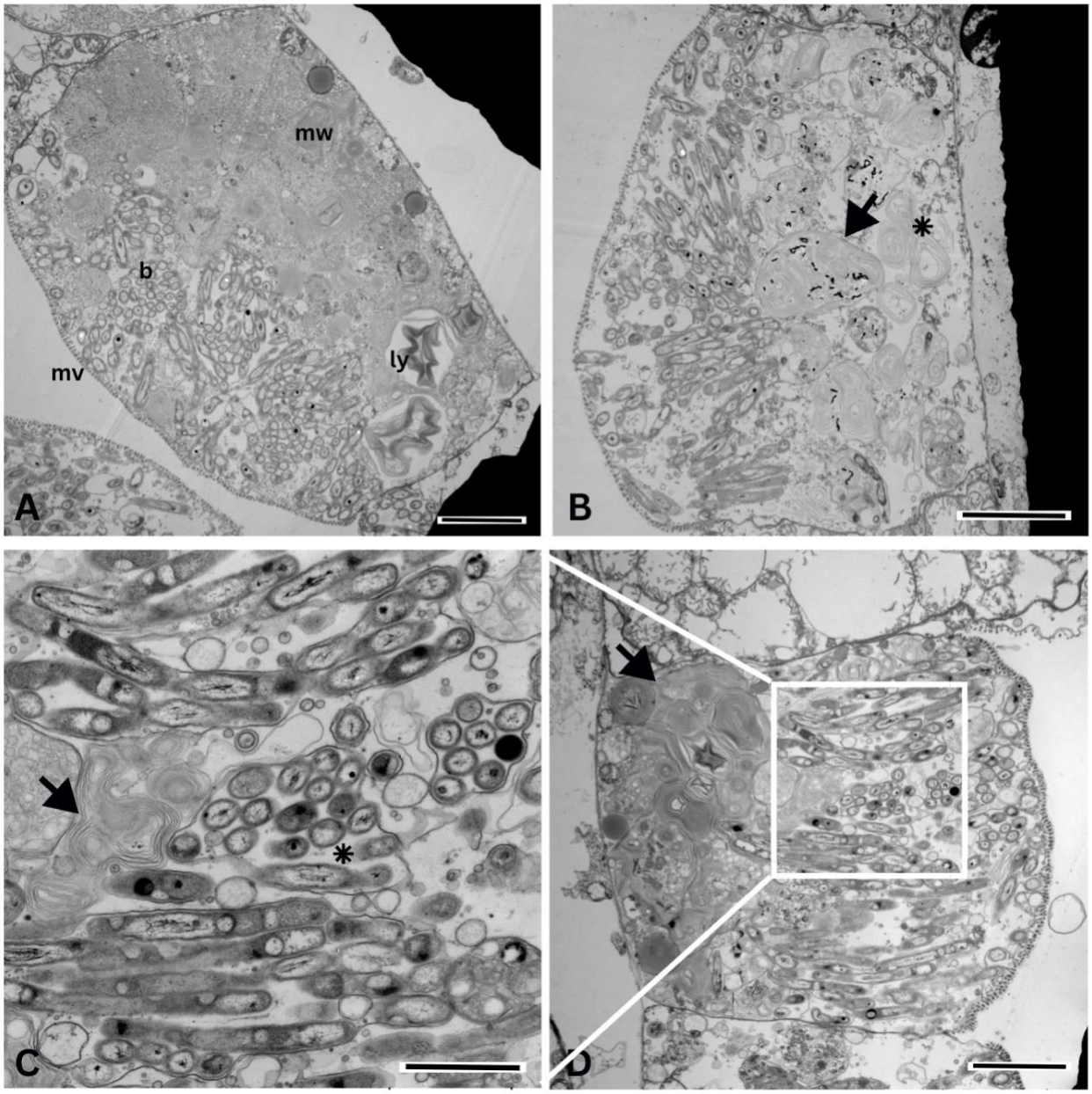
mw
b
mv
ly
A
B
C
D

Figure 12. TEM micrographs of bacteriocytes in gills of *Thyasira* cf. *gouldi* prepared for a previous study (Laurich et al., 2018). **A)** Bacteriocyte from a control specimen, maintained in sediment for 4 days. Abundant bacteria (b) are visible, retained by the microvillar border (mv). The cytoplasm contains abundant membrane whorls (mw) and irregular lysosomes (ly). **B)** Bacteriocyte from a control specimen, maintained in sediment for 2 days. Asterisk shows a membrane whorl with widely spaced membranes, while arrowhead shows a cluster of membrane whorls enveloped by a membrane. **C)**, inset of **D)** Specimen maintained in seawater with 2% thiosulphate and no added sediment for 1 day. Asterisk in C) shows a cluster of bacteria appearing to be surrounded by a membrane. Arrowheads in C) and D) show clusters of membrane whorls enveloped by a membrane. Scale bars: A, B, D = 5 μm; C = 2 μm.

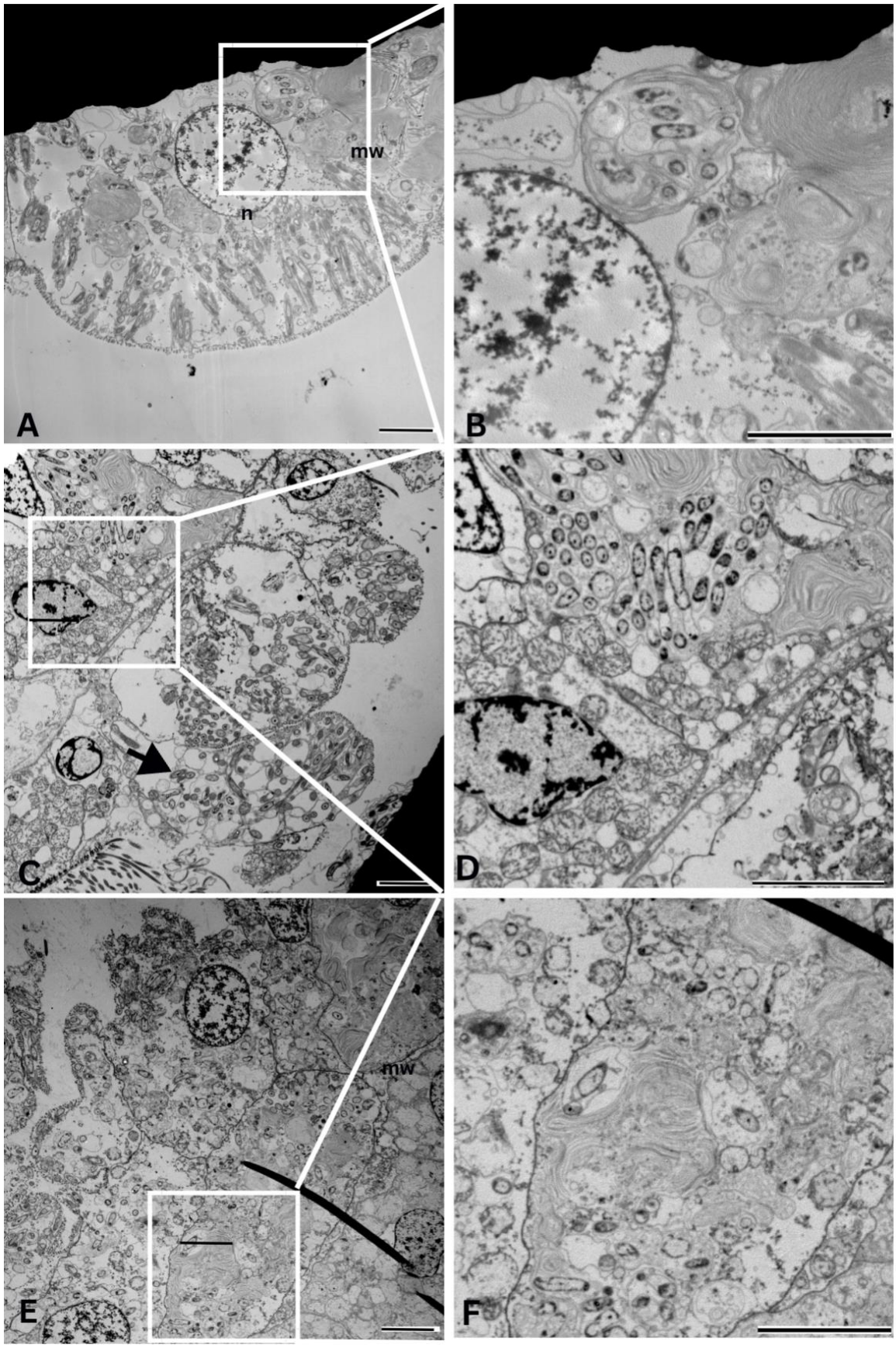
mw
n
A
B
C
D
mw
E
F

Figure 13. TEM micrographs of bacteriocytes in gills of *T*. cf. *gouldi* prepared for previous studies (Laurich et al. 2015, 2018). **A)** Specimen maintained in seawater with 2% thiosulphate and no added sediment for 12 hours. Membrane whorls (mw) are scattered throughout the cytoplasm. n: nucleus. **B)** Higher magnification of the bacteriocyte shown in **A)**, with membrane whorls and some visible bacteria. **C)** Specimen collected and immediately fixed in July 2012 (no treatment). Arrowhead shows groups of bacteria appearing to be surrounded by a membrane. **D)** Higher magnification of the bacteriocyte shown in C), with membrane whorls and some visible bacteria. **E)** Specimen collected and immediately fixed in October 2012 (no treatment), with clusters of membrane whorls (mw) visible. **F)** Higher magnification of the bacteriocyte shown in E), with membrane whorls and some visible bacteria. Scale bars: A, B, C, D, E, F = 5 μm

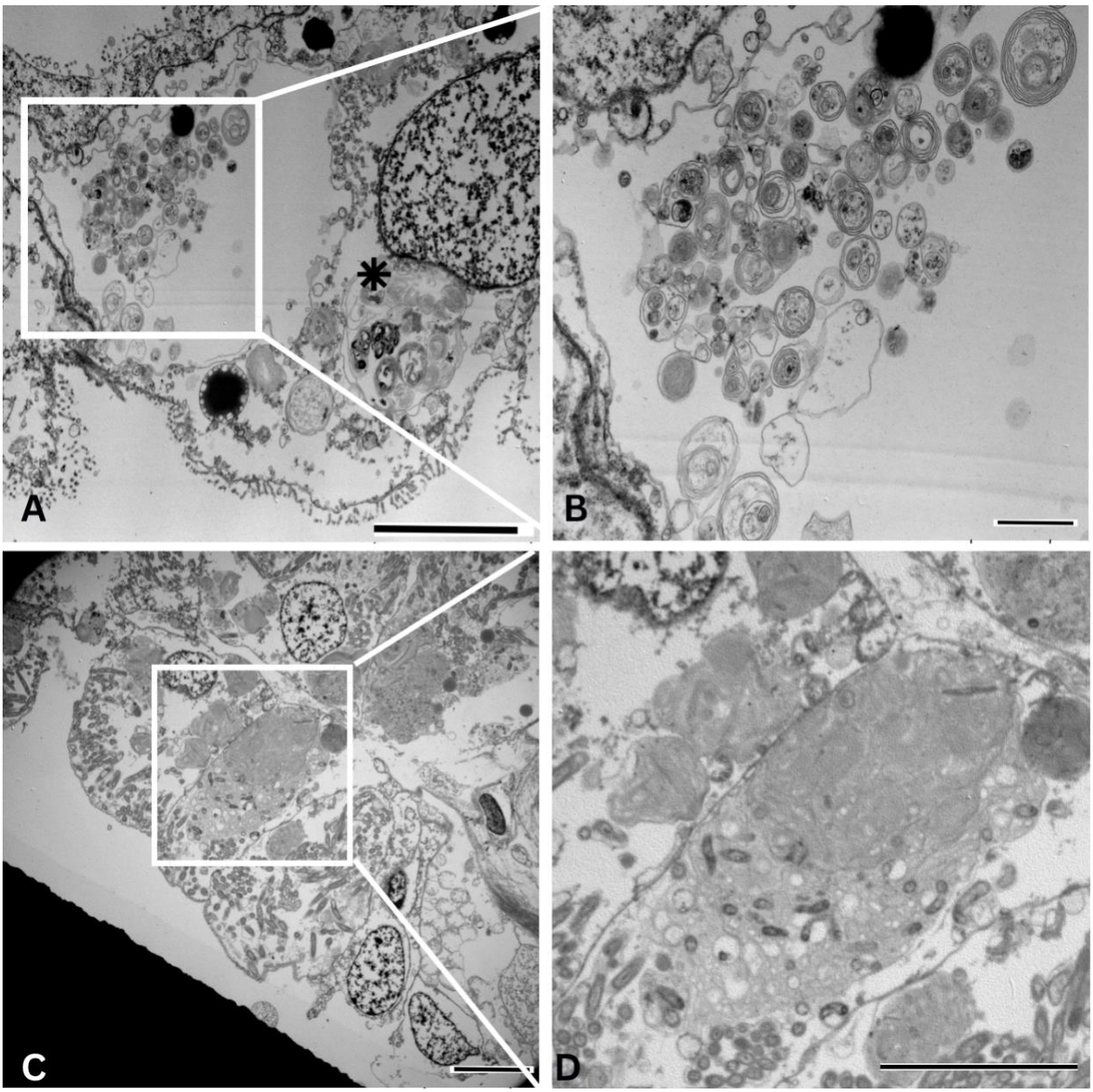
A
B
C
D

Figure 14. TEM micrographs of bacteriocytes in gills of *Thyasira* cf. *gouldi* prepared for an unpublished study (A, B), or for Laurich et al. (2015) (C, D). **A)** and inset **B)** Specimen maintained in filtered seawater (not in sediment) for 40 days and then placed in sediment for 16 days, showing numerous lysosomal bodies, some of which may include bacteria. Some inclusions seemed to contain bacteria that were undergoing degradation (asterisk). **C)** and **D)** Specimen collected in May 2012 and immediately fixed (no experimental maintenance). Bacterial symbionts are visible amongst microvilli. Membrane whorls at the apical end of the cell appear less tightly packed and include bacteria, while membrane whorls at the basal end are more tightly packed and electron dense, containing few to no apparent bacteria. Scale bars: A = 5 μm; B = 1 μm; C, D = 10 μm

Some membrane whorls included small, electron-dense inclusions, which in some cases appeared aligned as chains (i.e. within structure marked with **arrowhead** in Fig. 12B). Small inclusions of similar size appeared scattered within some of the larger membrane whorls (or clusters of whorls) having a high density of tightly-packed membranes with a more uniform electron density (**mw**, Fig. 11B).

The presence of membrane whorls of various morphologies was confirmed in specimens sampled and immediately fixed for electron microscopy in different months (April 2011, June 2011, August 2011, October 2011, December 2011, May 2012, July 2012, and October 2012). Similarly, membrane whorls were observed in specimens maintained in aquaria under different conditions (within sediments or directly in seawater, with or without the addition of thiosulphate). The inclusion of bacterial symbionts within some of the visible membrane whorl structures seemed to be consistent across bacteriocytes of specimens collected in different months, or following different experimental treatments. No further patterns with regards to membrane whorl morphology and either specimen sampling date or experimental treatment were evident.

Chapter 4: Discussion

Fluorescent staining and confocal microscopy of *Thyasira* cf. *gouldi* gills revealed a different perspective of the bacterial symbionts and gill filaments compared to how they are typically seen on TEM images. Due to the way that whole gills (or half-gills) are mounted on microscope slides (i.e. with frontal ends downwards), optical sectioning through whole-mounted gills generally provided views of filaments along an anterior-posterior plane, which differs from the frontal-abfrontal plane typically observed with TEM as a result of how gills are oriented in resin blocks upon embedding. Through the stacking of serial optical sections, confocal microscopy has enabled more holistic views of bacteriocyte cell structures. While confocal microscopy can help advance our understanding of host-symbiont relationships at the cellular level, some challenges remain with the consistency and reliability of fluorescence labelling.

4.1 Observation of bacteriocyte cellular structures using confocal microscopy, with limited evidence for phagocytosis and intracellular digestion

The bacteriocyte structures most clearly and consistently labeled by fluorescent probes in this study were the nuclei. I opted to use Prolong Gold antifade reagent mountant with DAPI as the final step in our protocols, allowing us to skip a wash step and combining nucleic acid staining with curing under the coverslip. Notably, gill cell nuclei appeared to occupy a larger amount of cellular space than is suggested by TEM imaging. In part, this may be due to a biased impression of the size of nuclei following ultra-thin sectioning for TEM, along planes that are likely to under-represent nuclear size (confocal sections are on the order of µm, compared to 70-100 nm for TEM). Additionally, because thyasirids were sampled in May, when symbiont populations are expected to be low, the entire bacteriocyte volume (including the extracellular space where symbionts are found) may have been relatively smaller than it tends to be in the

summer and fall months (Laurich et al., 2015), leading to the impression of abnormally large host nuclei. Estimates of the maximal size of nuclei based on confocal sections (approximately 10 μm; see Fig. 7A) corresponded to, or were slightly smaller than the largest nuclei observed on TEM images (see Fig. 13A).

Phalloidin was an effective marker of some elements of bacteriocyte cell membranes, notably the extremity of microvilli, which appeared as a thin border at the apical end of the cells (Fig. 7C, D). Microvilli are packed with bundles of F-actin (Cooper, 2000), to which the phalloidin could bind; the more evident labelling of microvilli compared to elsewhere within host cells might indicate a greater density of actin in the microvilli than elsewhere, or a greater ease of access of the phalloidin dye at the distal ends of cells. Some phalloidin staining was observed at the border of neighbouring bacteriocytes (Fig. 7C), allowing visualization of membrane boundaries, but this was relatively uncommon. The apparently irregular cell membrane located internally to the extracellular space that holds symbionts (see Fig. 11B) did not appear to be stained by phalloidin.

Since phagocytosis is driven by rearrangements of actin cytoskeleton to eventually engulf the symbiont and form a vacuole (Guo et al., 2023), I expected to see evidence of this process in the bacteriocytes of *Thyasira* cf. *gouldi* via phalloidin labelling. Phalloidin marked the phagocytotic uptake of bacteria in other studies, for example in investigations of neutrophils harvested from the blood of mice (Li et al., 2017). The lack of evident phalloidin staining in more central parts of bacteriocytes, where phagocytosis is expected to take place, may be due to inadequate penetration of the dye. Alternatively, it may indicate that little phagocytosis was taking place in those gills at the time of processing, that it happened too rapidly for effective

labelling, or that the concentration of actin around phagocytotic structures was not sufficient to allow clear detection.

I attempted to label acidic organelles, such as lysosomes and possibly phagolysosomes, using LysoTracker. While in some instances, background staining was considerable (Fig. 8A), a few possible lysosomes or phagolysosomes may have been observed (Fig. 8B). The putative lysosomes or phagolysosomes that were stained with LysoTracker were of small size (10 to 12 μm) and, notably, were rare within the gills observed. There was no evidence that the abundant membrane whorls that occupy a large fraction of the cytoplasm of bacteriocytes, and were observed in the TEMs of gill fragments (Fig. 11A, B), were stained with LysoTracker. There are several reasons LysoTracker may not have marked as many cellular structures as expected in *T.* cf. *gouldi* gill filament bacteriocytes. The protocols recommended by the supplier were developed for mammalian cells, and may not have been optimal for bivalve gill cells; however, at least two studies appeared to successfully label lysosomes using LysoTracker in bivalves, specifically in isolated hemocytes (Mateo et al., 2009), and more notably, in gill epithelial cells of the mussel *Bathymodiolus japonicus* (Tame et al., 2022). In *B. japonicus*, LysoTracker staining was evident in gill epithelial cells following 2 h and 24 h of incubation with *E. coli*, indicating lysis of phagocytosed exogenous bacteria, with the number of LysoTracker-labeled structures increasing with time (Tame et al., 2022). In *T.* cf. *gouldi* gills, a longer LysoTracker staining time might have resulted in a greater number of labeled structures. It is possible that when the staining took place, there was no digestion occurring (perhaps due to low symbiont abundance), or that the vast majority of phagosomes or phagolysosomes present were at later stages of digestion and no longer acidic. Guo et al. (2023) suggested that symbiont digestion takes place rapidly following their engulfment in the gills of another thyasirid clam with

extracellular symbionts, *Conchocele bisecta*. In the latter species, sequencing of the genome and comparison with other chemosymbiotic bivalves having endosymbionts provided evidence for expansion events in families of genes (or KEGG orthologs) involved with lysosome-mediated intracellular digestion and lysosome recycling; additionally, hydrolases such as cathepsins were highly expressed in *C. bisecta* gills (Guo et al., 2023). Future work should examine whether *T.* cf. *gouldi* gills show high expression of genes responsible for phagocytosis and lysosomal activity, to better assess the importance of symbiont uptake and digestion in the nutritional currency of these bivalves. Contrasting expression levels under different experimental conditions, such as through the manipulation of reduced sulfide concentrations, could indicate whether external factors might trigger symbiont digestion in *T.* cf. *gouldi* gills, as has been observed in mussels with intracellular symbionts (Wang et al., 2023).

The low prevalence of LysoTracker labelling in *T.* cf. *gouldi* gills might lead us to use caution in interpreting all membrane whorls as being sites of active symbiont digestion. In the mussel *Bathymodiolus azoricus*, which harbours endosymbionts within host vacuoles, and in which bacteriocytes contain large vesicles with membrane content resembling the membrane whorls of thyasirids, a study using enzyme cytochemistry provided little support for active lysosomal digestion of symbionts in bacteriocytes (Kádár et al., 2008). Interestingly, the absence of hydrolase activity within the *B. azoricus* cell structures assumed to be involved with intracellular digestion of symbionts led Kádár et al. (2008) to suggest that the term "lysosome" had been used incorrectly for those vesicles. Alternative modes of nutrient transfer apart from symbiont digestion, such as inter-membrane or vesicular transport (a form of 'milking'), should be considered in thyasirid bivalves.

4.2 Observation and live/dead state of bacterial symbionts

I know from Laurich et al. (2015) that there is a temporal variation in the abundance of symbionts in Bonne Bay thyasirids, with the abundance being highest in the fall and lowest in the spring. The samples collected for this study were obtained on 24 May 2022, and therefore I expected the bacterial symbiont abundance to be low in the specimens that were sampled. All gills examined over the course of this study (up to October 2022), through both confocal microscopy and TEM, had low symbiont numbers. The maintenance of thyasirids in aquaria for up to 5 months did not result in an increase in symbiont abundance, which would have been expected to occur under natural conditions, nor did it result in the elimination of symbionts.

In this study, DAPI was not effective for labelling symbionts, although it was expected to dimly stain bacteria (Biotum, 2022). The relatively low concentration of DNA in bacteria compared to host nuclei may have led to the ineffective symbiont staining. In other studies, DAPI was used to label symbionts in bivalve gills, notably in bathymodiolin mussels (e.g. Piquet et al., 2020, Tame et al., 2022). Symbionts are more abundant in the gill of bathymodiolins than in *Thyasira* cf. *gouldi*, which may partly explain this difference in staining efficiency. Alternative nucleic acid stains, such as SYBR Gold, may provide better results in labelling symbionts.

Initially, I intended to characterize the relative amount of active vs. total bacteria by contrasting those labeled by CTC (actively respiring bacteria) with those labeled by DAPI following fixation. CTC provided some indication that there were live, respiring bacteria in the gills of dissected thyasirids, likely in the expected location (apical end of bacteriocytes); the exact location of symbionts should be confirmed using phalloidin bound to another fluorescent dye, allowing phalloidin and CTC to be used concurrently. The abundance of CTC-labeled

bacteria was lower than the total number of symbionts present, as visualized by contrasting symbiont abundance in a half-gill prepared for TEM (Fig. 11) with the corresponding half-gill labeled with CTC and DAPI (online Z-stack). This discrepancy could indicate that some of the bacteria associated with bacteriocytes were dead, or not respiring at the time of processing. However, the very faint, inconclusive staining with PI in preparations does not enable a clear assessment of whether bacteria associated with bacteriocytes were dead or alive.

4.3 Membrane whorls and symbiont digestion

In the bacteriocytes of *Thyasira* cf. *gouldi* observed using TEM, apparent clusters of symbionts surrounded by a membrane might be early phagosomes, but this would need to be confirmed by verifying their three-dimensional morphology using different observational approaches (see Conclusions and Future Directions). On single 2D images of *T*. cf. *gouldi* bacteriocytes, inferring whether vacuole-like, symbiont-containing structures are truly intracellular or are obliquely sectioned invaginations of the cell membrane enveloping extracellularly-positioned symbionts is difficult due to highly the convoluted state of the cell membrane. On some TEM images (e.g. Fig. 13C), there seemed to be many distinct vacuoles containing a small number of symbionts. Confirming that these are truly phagosomes would require more detailed, three-dimensional reconstructions of structures within bacteriocytes.

In *Thyasira* cf. *gouldi* bacteriocytes, membrane whorls observed using TEM are consistent with the description of lysosomes as being electron dense and sometimes containing membrane whorls (Barral et al., 2021). Lysosomes are morphologically variable structures that have recently been recognized as playing a variety of roles in cells beyond catalysis, including nutrient sensing and cellular homeostasis (Bouhamdani et al., 2021). Rather than being simple, homogenous, single-purpose organelles, lysosomes are dynamic and can be broadly defined as

varying in cellular localization, enzymatic content and acidity (Barral et al., 2021). The cellular pathways leading to the degradation of phagocytosed materials involve interaction of terminal lysosomes (bearing the cargo of hydrolytic enzymes) and phagosomes (or late endosomes) through either fusion or "kiss-and-run" events (Bouhamdani et al., 2021). The result of this fusion is the formation of endolysosomes (here termed phagolysosomes), which are the site of hydrolase activity (Bright et al., 2016). Phagolysosomes are typically larger, acidic and catabolically active, whereas terminal lysosomes are smaller, less acidic and catabolically inactive (De Araujo et al., 2019). Terminal lysosomes appear as small, dense bodies on electron micrographs (Tjelle et al., 1996).

In the gills of *Thyasira* cf. *gouldi*, structures broadly defined as membrane whorls may represent a variety of stages in the pathway from phagocytosis to degradation. Structures that are more electron lucent and contain internalized symbionts could be interpreted as early phagolysosomes. Notably, many of the symbionts within membrane whorls appear intact, suggesting that catabolism may not have been taking place within those structures at the time of fixation. Only a few of the membrane whorls observed on TEM images appeared to have more degraded symbionts, which could represent hydrolase-active, later phagolysosomes (Fig. 14A). An apparently low rate of symbiont hydrolysis overall would be consistent with the results of the LysoTracker assays, which suggested that few of the bacteriocytes were actively digesting symbionts. Symbiont digestion in the gills of *T.* cf. *gouldi* may occur as relatively short-lived and somewhat infrequent events; remarkably, Guo et al. (2023) reported that symbiont digestion tends to be rapid in *C. bisecta* bacteriocytes. It is possible that the majority of the phagolysosomal structures (with internalized symbionts) typically observed in *T.* cf. *gouldi* gills are at the pre-digestive stage, potentially representing a readily available store of nutrients for

these clams. In the chemosymbiotic mussel *Bathymodiolus japonicus*, degradation of intracellular symbionts maintained within vacuoles (called symbiosomes) is regulated by the mechanistic target of rapamycin complex 1 (mTORC1), which is located on the lysosomal surface and regulates cell metabolism by sensing amino acids and sterols within lysosomes (Tame et al., 2023). It would be interesting to search for and eventually quantify transcripts of mTORC1 in the gills of *T.* cf. *gouldi* to explore whether it may be involved in symbiont degradation. mTORC1 activity can be assessed using in vitro or in vivo assays (Barral et al., 2021), which could be attempted in *T.* cf. *gouldi* gills.

In contrast, the (usually) more electron-dense structures that are most often located near the basal end of bacteriocytes could represent later, post-digestive stages of symbiont digestion, and might be best described as residual bodies. Notably, these structures have been found to contain undigested magnetosome nanoparticles (Dufour et al., 2014), suggesting they represent terminal stages of digestion. The localization of interpreted earlier phagolysosomes towards the apical end of cells, and of later stages (including residual bodies) near the basal end corresponds to previous descriptions (Barral et al., 2021).

Notably, few of the lysosomes observed appear to have a simple, spherical structure. Instead, they generally have a complex morphology (irregular shape, clustering of membrane whorls) and relatively large size, in contrast to the smaller, vesicular/spherical structures described in other cells (Araujo et al., 2019; Bouhamdani et al., 2021), which typically measure 200-600 nm in diameter (Barral et al., 2021). Notably, some lysosomes, including in dendritic cells (a type of immune cell), are considerably larger, highly branched and irregular and have been described as tubular lysosomes (Bohnert & Johnson, 2022). Tubular lysosomes may form an interconnected network spanning the cytoplasm, and this increased volume and surface area

has been proposed to play a role in increasing the holding capacity of lysosomes and the turnover of phagocytosed materials (Bohnert & Johnson, 2022). The possibility that the membrane whorls in *T.* cf. *gouldi* bacteriocytes may be akin to these tubular lysosomes is intriguing and merits further study.

Chapter 5: Conclusions and future directions

This thesis presents findings of research using various fluorescent stains and confocal microscopy to visualize the interaction between chemoautotrophic symbionts and gill epithelial cells of marine molluscs (Family: Thyasiridae). DAPI and phalloidin were consistent in their labelling of host nuclei and the microvillar layer, respectively. CTC appeared effective for labelling bacterial symbionts but could colocalize with phalloidin. Notably, CTC did not seem to label all symbionts present, suggesting that some of the symbionts may not have been actively respiring (at least during specimen processing). The LysoTracker dye sometimes yielded considerable background staining but appeared to effectively label a very small number of acidic organelles under the incubation conditions used. Propidium iodide was tested as a substitute for DAPI, but only very faint staining was observed.

Future work could focus on optimizing protocols for staining, and repeating attempts with symbiotic thyasirids collected in the fall months when symbionts are more abundant. For the specific labelling of symbionts, probes targeting gene sequences could be designed and employed, but would come with the disadvantage of requiring more complex Fluorescence In Situ Hybridization processing (and could preclude the combined use of live probes such as LysoTracker).

It remains unclear whether the lack of clear labelling of instances of bacterial engulfment via phalloidin, and the very low abundance of labeled acidic organelles in the gill epithelial cell by LysoTracker are indications of low rates of symbiont phagocytosis and digestion in *T*. cf. *gouldi*. Even if these results were accurate in reflecting low symbiont uptake and digestion rates, further studies should consider whether there would be seasonal differences in those processes, as well as any impacts due to aquarium maintenance. Alternative approaches to investigating phagocytosis and lysosomal activity in *T*. cf. *gouldi* gills, such as cytoenzymology (Kádár et al., 2008; Barral et al., 2021), host gene sequence and transcript analysis (Guo et al., 2023), lysosomal assays (Barral et al., 2021) or high-resolution, 3D scanning tools such as FIB-SEM (Heymann et al., 2006), which involves serial milling of blocks of embedded tissue with a focused beam of high-energy gallium ions interspersed with scanning electron microscope imaging, could provide useful insights on cellular and physiological processes linked to symbiosis in those bivalves.

References

Altamia, M. A., & Distel, D. L. (2022). Transport of symbiont-encoded cellulases from the gill to the gut of shipworms via the enigmatic ducts of Deshayes: A 174-year mystery solved. *Proceedings of the Royal Society B: Biological Sciences*, *289*(1986), 20221478. https://doi.org/10.1098/rspb.2022.1478

Ansorge, R., Romano, S., Sayavedra, L., Porras, M. Á. G., Kupczok, A., Tegetmeyer, H. E., Dubilier, N., & Petersen, J. (2019). Functional diversity enables multiple symbiont strains to coexist in deep-sea mussels. *Nature Microbiology*, *4*(12), 2487–2497. https://doi.org/10.1038/s41564-019-0572-9

Barral, D. C., Staiano, L., Guimas Almeida, C., Cutler, D. F., Eden, E. R., Futter, C. E., Galione, A., Marques, A. R. A., Medina, D. L., Napolitano, G., Settembre, C., Vieira, O. V., Aerts, J. M. F. G., Atakpa-Adaji, P., Bruno, G., Capuozzo, A., De Leonibus, E., Di Malta, C., Escrevente, C., … Seabra, M. C. (2022). Current methods to analyze lysosome morphology, positioning, motility and function. *Traffic*, *23*(5), 238–269. https://doi.org/10.1111/tra.12839

Bartosch, S., Mansch, R., Knötzsch, K., & Bock, E. (2003). CTC staining and counting of actively respiring bacteria in natural stone using confocal laser scanning microscopy. *Journal of Microbiological Methods*, *52*(1), 75–84. https://doi.org/10.1016/S0167-7012(02)00133-1

Batstone, R. T., & Dufour, S. C. (2016). Closely related thyasirid bivalves associate with multiple symbiont phylotypes. *Marine Ecology*, *37*(5), 988–997. https://doi.org/10.1111/maec.12310

Batstone, R. T., Laurich, J. R., Salvo, F., & Dufour, S. C. (2014). Divergent chemosymbiosis-related characters in *Thyasira* cf. *gouldi* (Bivalvia: Thyasiridae). *PLoS ONE*, *9*(3), e92856. https://doi.org/10.1371/journal.pone.0092856

Betcher, M. A., Fung, J. M., Han, A. W., O'Connor, R., Seronay, R., Concepcion, G. P., Distel, D. L., & Haygood, M. G. (2012). Microbial Distribution and Abundance in the Digestive System of Five Shipworm Species (Bivalvia: Teredinidae). *PLoS ONE*, *7*(9), e45309. https://doi.org/10.1371/journal.pone.0045309

Biotium. (2022, May 4). Protocol: Staining cells with Hoechst or DAPI nuclear stains. Biotium. https://biotium.com/tech-tips/protocol-staining-cells-with-hoechst-or-dapi-nuclear-stains/#:~:text=Hoechst%20and%20DAPI%20stain%20bacteria,more%20brightly%20than%20live%20cells.

Bohnert, K. A., & Johnson, A. E. (2022). Branching off: new insight into lysosomes as tubular organelles. *Frontiers in Cell and Developmental Biology*, *10*, 863922. https://doi.org/10.3389/fcell.2022.863922

Boulos, L., Prévost, M., Barbeau, B., Coallier, J., & Desjardins, R. (1999). LIVE/DEAD® BacLight™: Application of a new rapid staining method for direct enumeration of viable and total bacteria in drinking water. *Journal of Microbiological Methods*, *37*(1), 77–86. https://doi.org/10.1016/S0167-7012(99)00048-2

Bouhamdani, N., Comeau, D., & Turcotte, S. (2021). A compendium of information on the lysosome. *Frontiers in Cell and Developmental Biology*, *9*, 798262. https://doi.org/10.3389/fcell.2021.798262

Bright, M., & Bulgheresi, S. (2010). A complex journey: Transmission of microbial symbionts. *Nature Reviews Microbiology*, *8*(3), 218–230. https://doi.org/10.1038/nrmicro2262

Bright, N. A., Davis, L. J., & Luzio, J. P. (2016). Endolysosomes are the principal intracellular sites of acid hydrolase activity. *Current Biology*, *26*(17), 2233–2245. https://doi.org/10.1016/j.cub.2016.06.046

Cappello, S., Russo, D., Santisi, S., Calogero, R., Gertler, C., Crisafi, F., De Domenico, M., & Yakimov, M. M. (2012). Presence of hydrocarbon-degrading bacteria in the gills of mussel *Mytilus galloprovincialis* in a contaminated environment: A mesoscale simulation study. *Chemistry and Ecology*, *28*(3), 239–252. https://doi.org/10.1080/02757540.2011.639768

Childress, J. J., Fisher, C. R., Brooks, J. M., Kennicutt, M. C., Bidigare, R., & Anderson, A. E. (1986). A methanotrophic marine molluscan (Bivalvia, Mytilidae) symbiosis: mussels fueled by gas. *Science*, *233*(4770), 1306–1308. https://doi.org/10.1126/science.233.4770.1306

Collazo, A., Bricaud, O., & Desai, K. (2005). Use of confocal microscopy in comparative studies of vertebrate morphology. In *Methods in Enzymology* (Vol. 395, pp. 521–543). Elsevier. https://doi.org/10.1016/S0076-6879(05)95027-1

Cooper GM. The Cell: A Molecular Approach. 2nd edition. Sunderland (MA): Sinauer Associates; 2000. Lysosomes. Available from: https://www.ncbi.nlm.nih.gov/books/NBK9953/

Créach, V., Baudoux, A.-C., Bertru, G., & Rouzic, B. L. (2003). Direct estimate of active bacteria: CTC use and limitations. *Journal of Microbiological Methods*, *52*(1), 19–28. https://doi.org/10.1016/S0167-7012(02)00128-8

Cruz-Flores, R., & Cáceres-Martínez, J. (2020). Rickettsiales-like organisms in bivalves and marine gastropods: A review. *Reviews in Aquaculture*, *12*(4), 2010–2026. https://doi.org/10.1111/raq.12419

Dando, P R, Spiro, B. (1993). Varying nutritional dependence of the thyasirid bivalves *Thyasira sarsi* and *T. equalis* on chemoautotrophic symbiotic bacteria, demonstrated by isotope ratios of tissue carbon and shell carbonate. *Marine Ecology Progress Series*, *92*(1/2), 151–158. http://www.jstor.org/stable/24832625

De Araujo, M. E. G., Liebscher, G., Hess, M. W., & Huber, L. A. (2020). Lysosomal size matters. *Traffic*, *21*(1), 60–75. https://doi.org/10.1111/tra.12714

Decker, C., Zorn, N., Le Bruchec, J., Caprais, J. C., Potier, N., Leize-Wagner, E., Lallier, F. H., Olu, K., & Andersen, A. C. (2017). Can the hemoglobin characteristics of vesicomyid clam species influence their distribution in deep-sea sulfide-rich sediments? A case study in the Angola Basin. *Deep Sea Research Part II: Topical Studies in Oceanography*, *142*, 219–232. https://doi.org/10.1016/j.dsr2.2016.11.009

DesMarais, V., Eddy, R. J., Sharma, V. P., Stone, O., & Condeelis, J. S. (2019). Optimizing leading edge F-actin labeling using multiple actin probes, fixation methods and imaging modalities. *BioTechniques*, *66*(3), 113–119. https://doi.org/10.2144/btn-2018-0112

Deshpande, O. A., & Wadhwa, R. (2024). Phagocytosis. In *StatPearls*. StatPearls Publishing. http://www.ncbi.nlm.nih.gov/books/NBK556043/

Dubilier, N., Bergin, C. & Lott, C. Symbiotic diversity in marine animals: the art of harnessing chemosynthesis. *Nat Rev Microbiol* **6**, 725–740 (2008). https://doi.org/10.1038/nrmicro1992

Dufour, S. C. (2005). Gill anatomy and the evolution of symbiosis in the bivalve family Thyasiridae. *The Biological Bulletin*, *208*(3), 200–212. https://doi.org/10.2307/3593152

Dufour, S. C., Laurich, J. R., Batstone, R. T., McCuaig, B., Elliott, A., & Poduska, K. M. (2014). Magnetosome-containing bacteria living as symbionts of bivalves. *The ISME Journal*, *8*(12), 2453–2462. https://doi.org/10.1038/ismej.2014.93

Fujiwara, Y., Kato, C., Masui, N., Fujikura, K., & Kojima, S. (2001). Dual symbiosis in the cold-seep thyasirid clam *Maorithyas hadalis* from the hadal zone in the Japan Trench, western Pacific. *Marine Ecology Progress Series*, *214*, 151–159. https://doi.org/10.3354/meps214151

Giere, O. (1985). Structure and position of bacterial endosymbionts in the gill filaments of Lucinidae from Bermuda (Mollusca, Bivalvia). *Zoomorphology*, *105*(5), 296–301. https://doi.org/10.1007/BF00312060

Guo, Y., Meng, L., Wang, M., Zhong, Z., Li, D., Zhang, Y., Li, H., Zhang, H., Seim, I., Li, Y., Jiang, A., Ji, Q., Su, X., Chen, J., Fan, G., Li, C., & Liu, S. (2023). Hologenome analysis reveals independent evolution to chemosymbiosis by deep-sea bivalves. *BMC Biology*, *21*(1), 51. https://doi.org/10.1186/s12915-023-01551-z

Gros, O. & Gaill, F. (2007). Extracellular bacterial association in gills of "wood mussels". *Cahiers de Biologie Marine, 48*, 103-109.

Hentschel, U., Steinert, M., & Hacker, J. (2000). Common molecular mechanisms of symbiosis and pathogenesis. *Trends in Microbiology*, *8*(5), 226–231. https://doi.org/10.1016/S0966-842X(00)01758-3

Heymann, J. A. W., Hayles, M., Gestmann, I., Giannuzzi, L. A., Lich, B., & Subramaniam, S. (2006). Site-specific 3D imaging of cells and tissues with a dual beam microscope. *Journal of Structural Biology*, *155*(1), 63–73. https://doi.org/10.1016/j.jsb.2006.03.006

Hughes, I. V., & Girguis, P. R. (2023). A molluscan class struggle: Exploring the surprisingly uneven distribution of chemosymbiosis among two major mollusk groups. *Frontiers in Marine Science*, *10*, 1167803. https://doi.org/10.3389/fmars.2023.1167803

Kádár, E., Davis, S. A., & Lobo-da-Cunha, A. (2008). Cytoenzymatic investigation of intracellular digestion in the symbiont-bearing hydrothermal bivalve *Bathymodiolus azoricus*. *Marine Biology*, *153*(5), 995–1004. https://doi.org/10.1007/s00227-007-0872-0

Kapuscinski, J. (1995). DAPI: A DNA-specific fluorescent probe. *Biotechnic & Histochemistry*, *70*(5), 220–233. https://doi.org/10.3109/10520299509108199

Karapunar, B., Werner, W., Fürsich, F. T., & Nützel, A. (2020): Predatory drill holes in the oldest thyasirid bivalve, from the Lower Jurassic of South Germany. *Lethaia*, *54,* 229–244.

Keuning, R., Schander, C., Kongsrud, J. A., & Willassen, E. (2011). Ecology of twelve species of Thyasiridae (Mollusca: Bivalvia). *Marine Pollution Bulletin*, *62*(4), 786–791. https://doi.org/10.1016/j.marpolbul.2011.01.004

König, S., Gros, O., Heiden, S. E., Hinzke, T., Thürmer, A., Poehlein, A., Meyer, S., Vatin, M., Mbéguié-A-Mbéguié, D., Tocny, J., Ponnudurai, R., Daniel, R., Becher, D., Schweder, T., & Markert, S. (2016). Nitrogen fixation in a chemoautotrophic lucinid symbiosis. *Nature Microbiology*, *2*(1), 16193. https://doi.org/10.1038/nmicrobiol.2016.193

Laurich, J. R., Batstone, R. T., & Dufour, S. C. (2015). Temporal variation in chemoautotrophic symbiont abundance in the thyasirid bivalve *Thyasira* cf. *gouldi*. *Marine Biology*, *162*(10), 2018–2028. https://doi.org/10.1007/s00227-015-2727-4

Laurich, J. R., Dove, R., Paillard, C., & Dufour, S. C. (2018). Life and death in facultative chemosymbioses: Control of bacterial population dynamics in the Thyasiridae. *Symbiosis*, *75*(2), 123–133. https://doi.org/10.1007/s13199-017-0525-0

Le Pennec, M., Diouris, M., & Herry, A. (1988). Endocytosis and lysis of bacteria in gill epithelium of *Bathymodiolus thermophilus, Thyasira flexuosa* and *Lucinella divaricata* (Bivalve, Molluscs). *Journal of Shellfish Research*, *7*(3), 483–489.

Li, C., Wang, M., Wang, H., Zhou, L., Zhong, Z., Chen, H., & Sun, Y. (2023a). Symbioses from cold seeps. In D. Chen & D. Feng (Eds.), *South China Sea Seeps* (pp. 89–113). Springer Nature Singapore. https://doi.org/10.1007/978-981-99-1494-4_6

Li, Y., He, X., Lin, Y., Li, Y., Kamenev, G. M., Li, J., Qiu, J., & Sun, J. (2023b). Reduced chemosymbiont genome in the methane seep thyasirid and the cooperated metabolisms in the

holobiont under anaerobic sediment. *Molecular Ecology Resources*, *23*(8), 1853–1867. https://doi.org/10.1111/1755-0998.13846

Li, Z., Jiao, Y., Fan, E. K., Scott, M. J., Li, Y., Li, S., Billiar, T. R., Wilson, M. A., Shi, X., & Fan, J. (2017). Aging-impaired filamentous actin polymerization signaling reduces alveolar macrophage phagocytosis of bacteria. *The Journal of Immunology*, *199*(9), 3176–3186. https://doi.org/10.4049/jimmunol.1700140

Mariño, J., Augustine, S., Dufour, S. C., & Hurford, A. (2019). Dynamic Energy Budget theory predicts smaller energy reserves in thyasirid bivalves that harbour symbionts. *Journal of Sea Research*, *143*, 119–127. https://doi.org/10.1016/j.seares.2018.07.015

Mateo, D., Spurmanis, A., Siah, A., Araya, M., Kulka, M., Berthe, F., Johnson, G., & Greenwood, S. (2009). Changes induced by two strains of *Vibrio splendidus* in haemocyte subpopulations of *Mya arenaria*, detected by flow cytometry with LysoTracker. *Diseases of Aquatic Organisms*, *86*, 253–262. https://doi.org/10.3354/dao02121

McCuaig, B., Liboiron, F., & Dufour, S. C. (2017). The bivalve *Thyasira* cf. *gouldi* hosts chemoautotrophic symbiont populations with strain level diversity. *PeerJ*, *5*, e3597. https://doi.org/10.7717/peerj.3597

MolluscaBase eds. (2024). MolluscaBase. Thyasiridae Dall, 1900 (1895). Accessed through: World Register of Marine Species at: https://www.marinespecies.org/aphia.php?p=taxdetails&id=219 on 2024-01-20

Oliver, G. (2014). "TUBULAR GILLS" Extreme gill modification in the Thyasiroidea with the description of *Ochetoctena tomasi* gen. et sp. nov. (Bivalvia: Thyasiroidea). *Zoosystematics and Evolution*, *90*(2), 121–132. https://doi.org/10.3897/zse.90.8323

Passos, F. D., De Lima Curi Meserani, G., & Gros, O. (2007). Structural and ultrastructural analysis of the gills in the bacterial-bearing species *Thyasira falklandica* (Bivalvia, Mollusca). *Zoomorphology*, *126*(3), 153–162. https://doi.org/10.1007/s00435-007-0034-4

Petersen, J. M., Kemper, A., Gruber-Vodicka, H., Cardini, U., Van Der Geest, M., Kleiner, M., Bulgheresi, S., Mußmann, M., Herbold, C., Seah, B. K. B., Antony, C. P., Liu, D., Belitz, A., & Weber, M. (2016). Chemosynthetic symbionts of marine invertebrate animals are capable of nitrogen fixation. *Nature Microbiology*, *2*(1), 16195. https://doi.org/10.1038/nmicrobiol.2016.195

Petersen, J. M., Zielinski, F. U., Pape, T., Seifert, R., Moraru, C., Amann, R., Hourdez, S., Girguis, P. R., Wankel, S. D., Barbe, V., Pelletier, E., Fink, D., Borowski, C., Bach, W., & Dubilier, N. (2011). Hydrogen is an energy source for hydrothermal vent symbioses. *Nature*, *476*(7359), 176–180. https://doi.org/10.1038/nature10325

Piquet, B., Lallier, F. H., André, C., Shillito, B., Andersen, A. C., & Duperron, S. (2020). Regionalized cell proliferation in the symbiont-bearing gill of the hydrothermal vent mussel *Bathymodiolus azoricus*. *Symbiosis*, *82*(3), 225–233. https://doi.org/10.1007/s13199-020-00720-w

Piquet B., Le Panse S., Lallier F.H., Duperron S., & Andersen A.C. (2022). "There and back again" - Ultrastructural changes in the gills of Bathymodiolus vent-mussels during symbiont loss: Back to a regular filter- feeding epidermis. Front. Mar. Sci. 9:968331. doi: 10.3389/fmars.2022.968331

Philippi R. 1845. Bemerkungen über die Mollusken-Fauna von Massachusetts. *Zeitschrift für Malakozoologie 1845*, 68-79.

Powell, M. A., & Somero, G. N. (1985). Sulfide oxidation occurs in the animal tissue of the gutless clam, *Solemya reidi*. *The Biological Bulletin*, *169*(1), 164–181. https://doi.org/10.2307/1541396

Rodriguez, G. G., Phipps, D., Ishiguro, K., & Ridgway, H. F. (1992). Use of a fluorescent redox probe for direct visualization of actively respiring bacteria. *Applied and Environmental Microbiology*, *58*(6), 1801–1808. https://doi.org/10.1128/aem.58.6.1801-1808.1992

Rosenberg, M., Azevedo, N. F., & Ivask, A. (2019). Propidium iodide staining underestimates viability of adherent bacterial cells. *Scientific Reports*, *9*(1), 6483. https://doi.org/10.1038/s41598-019-42906-3

Shipway, J. R., Altamia, M. A., Haga, T., Velásquez, M., Albano, J., Dechavez, R., Concepcion, G. P., Haygood, M. G., & Distel, D. L. (2018). Observations on the life history and geographic range of the giant chemosymbiotic shipworm *Kuphus polythalamius* (Bivalvia: Teredinidae). *The Biological Bulletin*, *235*(3), 167–177. https://doi.org/10.1086/700278

Sigma Aldrich . (n.d.). 5-cyano-2,3-di-(p-tolyl)tetrazolium chloride. Accessed through Sigma Aldrich at: https://www.sigmaaldrich.com/CA/en/product/sigma/94498\ on September 15, 2022.

Sogin, E. M., Kleiner, M., Borowski, C., Gruber-Vodicka, H. R., & Dubilier, N. (2021). Life in the dark: phylogenetic and physiological diversity of chemosynthetic symbioses. *Annual Review of Microbiology*, *75*(1), 695–718. https://doi.org/10.1146/annurev-micro-051021-123130

Sogin, E. M., Leisch, N., & Dubilier, N. (2020). Chemosynthetic symbioses. *Current Biology*, *30*(19), R1137–R1142. https://doi.org/10.1016/j.cub.2020.07.050

Southward, E. C. (1986). Gill symbionts in thyasirids and other bivalve molluscs. *Journal of the Marine Biological Association of the United Kingdom*, *66*(4), 889–914. https://doi.org/10.1017/S0025315400048517

Tame, A., Maruyama, T., Ikuta, T., Chikaraishi, Y., Ogawa, N. O., Tsuchiya, M., Takishita, K., Tsuda, M., Hirai, M., Takaki, Y., Ohkouchi, N., Fujikura, K., & Yoshida, T. (2023). MTORC1

regulates phagosome digestion of symbiotic bacteria for intracellular nutritional symbiosis in a deep-sea mussel. *Science Advances*, *9*(34), eadg8364. https://doi.org/10.1126/sciadv.adg8364

Tame, A., Maruyama, T., & Yoshida, T. (2022). Phagocytosis of exogenous bacteria by gill epithelial cells in the deep-sea symbiotic mussel *Bathymodiolus japonicus*. *Royal Society Open Science*, *9*(5), 211384. https://doi.org/10.1098/rsos.211384

Taylor, J.D., & Glover, E.A. (2010). Chemosymbiotic Bivalves. In: Kiel, S. (eds) The Vent and Seep Biota. Topics in Geobiology, vol 33. Springer, Dordrecht. https://doi.org/10.1007/978-90-481-9572-5_5

Thermo Fisher Scientific - US. (n.d.-a). Alexa FluorTM 488 Phalloidin. Accessed from Thermo Fisher Scientific - US. https://www.thermofisher.com/order/catalog/product/A12379?SID=srch-srp-A12379 on September 15, 2022.

Thermo Fisher Scientific - US. (n.d.). LysoTrackerTM Deep Red. Accessed from Thermo Fisher Scientific - US. https://www.thermofisher.com/order/catalog/product/L12492?gclid=Cj0KCQjwyLGjBhDKARIsAFRNgW-Qcj4qwfl9Qw8a5xxgL6r9M76MBYVxlTkP1zdDS4t7GXW-i7cfkBoaAiFtEALw_wcB&ef_id=Cj0KCQjwyLGjBhDKARIsAFRNgW-Qcj4qwfl9Qw8a5xxgL6r9M76MBYVxlTkP1zdDS4t7GXW-i7cfkBoaAiFtEALw_wcB%3AG%3As&s_kwcid=AL%213652%213%21447292198736%21%21%21g%21%21%2110506731179%21109642167491&cid=bid_pca_iva_r01_co_cp1359_pjt0000_bid00000_0se_gaw_dy_pur_con on September 15, 2022.

Thermo Fisher Scientific - US. (n.d.-c). ProlongTM Gold Antifade Mountant with DNA Stain Dapi. Accessed from Thermo Fisher Scientific - US.

https://www.thermofisher.com/order/catalog/product/P36935?SID=srch-hj-P36935 on September 15, 2022.

Tjelle, T. E., Brech, A., Juvet, L. K., Griffiths, G., & Berg, T. (1996). Isolation and characterization of early endosomes, late endosomes and terminal lysosomes: Their role in protein degradation. *Journal of Cell Science*, *109*(12), 2905–2914. https://doi.org/10.1242/jcs.109.12.2905

Vetter, R. D., & Fry, B. (1998). Sulfur contents and sulfur-isotope compositions of thiotrophic symbioses in bivalve molluscs and vestimentiferan worms. *Marine Biology*, *132*(3), 453–460. https://doi.org/10.1007/s002270050411

Wang, H., He, K., Zhang, H., Zhang, Q., Cao, L., Li, J., Zhong, Z., Chen, H., Zhou, L., Lian, C., Wang, M., Chen, K., Qian, P.-Y., & Li, C. (2023). *Deciphering deep-sea chemosynthetic symbiosis by single-nucleus RNA- sequencing*. *eLife.* https://doi.org/10.7554/eLife.88294.1

Weiss, G., & Schaible, U. E. (2015). Macrophage defense mechanisms against intracellular bacteria. *Immunological Reviews*, *264*(1), 182–203. https://doi.org/10.1111/imr.12266

Wentrup, C., Wendeberg, A., Huang, J. Y., Borowski, C., & Dubilier, N. (2013). Shift from widespread symbiont infection of host tissues to specific colonization of gills in juvenile deep-sea mussels. *The ISME Journal*, *7*(6), 1244–1247. https://doi.org/10.1038/ismej.2013.5

Zanzerl, H., & Dufour, S.C. (2018) The burrowing behaviour of symbiotic and asymbiotic thyasirid bivalves. *Journal of Conchology 42,* 299-308.

Zanzerl, H., Salvo, F., Jones, S. W., & Dufour, S. C. (2019). Feeding strategies in symbiotic and asymbiotic thyasirid bivalves. *Journal of Sea Research*, *145*, 16–23. https://doi.org/10.1016/j.seares.2018.12.005

Appendices

Appendix A – Sample processing details for the thyasirid gills examined with confocal microscopy or transmission electron microscopy in the present study.

Clam	Size (mm)	Specimen #	Gill #	Date dissected & stained	Stains used	TEM	CTC (4 hours)	Lyso-tracker	4% formal.	0.1% Triton X	PI (5 min)	Phalloidin (20 mins)	DAPI	Date imaged	Figure #
Parathyasira	4	1	1,2	30-May-22	DAPI				x	x			x		
Parathyasira	5	2	1,2	01-Jun-22	DAPI				x	x					
Parathyasira	6	3	1,2	06-Jun-22	DAPI + phalloidin				x	x		x	x	07-Jun-22	
symbiotic	5	4	1,2	08-Jun-22	DAPI + phalloidin				x	x		x	x	09-Jun-22	6B, 6D
symbiotic	5	5	1,2	13-Jun-22	DAPI + phalloidin				x	x		x	x	13-Jun-22	6C
symbiotic	3.5	6	1	14-Jun-22	DAPI + phalloidin + lysotracker			x	x	x		x	x	15-Jun-22	
symbiotic	3.5	6	2	14-Jun-22	DAPI + phalloidin				x	x		x	x	15-Jun-22	
symbiotic	3.5	7	1	15-Jul-22	CTC + DAPI (2hrs)		x (2h)		x	x			x	25-Jul-22	
symbiotic	3.5	7	2	15-Jul-22	CTC + DAPI (4hrs)		x		x	x			x	25-Jul-22	
symbiotic	3.5	7	1	15-Jul-22	CTC (2hrs)		x (2hrs)		x	x				25-Jul-22	
symbiotic	3.5	7	2	15-Jul-22	CTC (4hrs)		x		x	x				25-Jul-22	

Clam	Size (mm)	Specimen #	Gill #	Date dissected & stained	Stains used	TEM	CTC (4 hours)	Lyso tracker	4% formal.	0.1% Triton X	PI (5 min)	Phalloidin (20 mins)	DAPI	Date imaged	Figure #
asymbiotic	5	8	2	26-Jul-22	CTC (control)		x		x	x				28-Jul-22	
asymbiotic	2	9	1	01-Aug-22	CTC + DAPI (4hrs)		x		x	x			x	04-Aug-22	8D
asymbiotic	2	9	2	01-Aug-22	CTC + DAPI + phalloidin		x		x	x		x	x	04-Aug-22	
symbiotic	4.5	10	1	04-Aug-22	CTC + DAPI (4hrs)		x		x	x			x	08-Aug-22	
symbiotic	4.5	10	2	04-Aug-22	CTC + DAPI + phalloidin		x		x	x		x	x	12-Aug-22	8A, 8B
symbiotic	4	11	1	12-Aug-22	Fixed in 2.5% glut	x			x	x					
symbiotic	4	11	2	12-Aug-22	CTC (4hrs)		x		x	x				01-Sep-22	
symbiotic	4	12	1	23-Aug-22	Fixed in 2.5% glut	x			x						
symbiotic	4	12	2 (half)	23-Aug-22	CTC + DAPI + phalloidin		x		x	x		x		01-Sep-22	8C
symbiotic	4	12	2 (half)	23-Aug-22	PI + phalloidin + DAPI				x	x	x	x	x	01-Sep-22	9C
symbiotic	4	13	1	07-Sep-22	PI after fixing then perm				x	x	x (after fix then perm)			12-Sep-22	9D,9B

Clam	Size (mm)	Specimen #	Gill #	Date dissected & stained	Stains used	TEM	CTC (4 hours)	Lyso tracker	4% formal.	0.1% Triton X	PI (5 min)	Phalloidin (20 min)	DAPI	Date imaged	Figure #
symbiotic	4	14	1(half)	26-Sep-22	Lysotracker + DAPI			x	x	x			x	29-Sep-22	
symbiotic	4	14	1(half)	26-Sep-22	Fixed in 2.5% glut	x			x						
symbiotic	4	14	2 (half)	26-Sep-22	CTC + DAPI (4hrs)		x		x	x			x	29-Sep-22	6A
symbiotic	4	14	2 (half)	26-Sep-22	Fixed in 2.5% glut	x			x						
symbiotic	4	15	1(half)	12-Oct-22	Fixed in 2.5% glut	x			x						
symbiotic	4	15	2 (half)	12-Oct-22	Fixed in 2.5% glut	x			x					19-May-23	11
symbiotic	4	15	1(half)	12-Oct-22	Lysotracker + DAPI			x	x	x			x	18-Oct-22	7A
symbiotic	4	15	2(half)	12-Oct-22	CTC + DAPI		x		x	x			x		
symbiotic	4	16	1(half)	12-Oct-22	Fixed in 2.5% glut	x			x						
symbiotic	4	16	2(half)	12-Oct-22	Fixed in 2.5% glut	x			x						
symbiotic	4	16	1(half)	12-Oct-22	Lysotracker + DAPI			x	x	x			x	29-Sep-22	7B

Clam	Size (mm)	Specimen #	Gill #	Date dissected & stained	Stains used	TEM	CTC (4 hours)	Lyso tracker	4% formal.	0.1% Triton X	PI (5 min)	Phalloidin (20 min)	DAPI	Date imaged	Figure #
symbiotic	3	17	1(half)	12-Oct-22	Fixed in 2.5% glut	x			x						
symbiotic	3	17	2 (half)	12-Oct-22	Fixed in 2.5% glut	x			x						
symbiotic	3	17	1(half)	12-Oct-22	Lysotracker + DAPI			x	x	x			x		
symbiotic	3	17	2 (half)	12-Oct-22	CTC + DAPI (4hrs)		x		x	x			x	10-Nov-22	8E
symbiotic	3	18	1(half)	12-Oct-22	Fixed in 2.5% glut	x			x						
symbiotic	3	18	2 (half)	12-Oct-22	Fixed in 2.5% glut	x			x						
symbiotic	3	18	1(half)	12-Oct-22	Lysotracker + DAPI			x	x	x			x		
symbiotic	3	18	2 (half)	12-Oct-22	CTC + DAPI (4hrs)		x		x	x			x		
symbiotic	3	19	1(half)	12-Oct-22	Fixed in 2.5% glut	x			x						
symbiotic	3	19	2 (half)	12-Oct-22	Fixed in 2.5% glut	x			x						

Clam	Size (mm)	Specimen #	Gill #	Date dissected & stained	Stains used	TEM	CTC (4 hours)	Lyso tracker	4% formal.	0.1% Triton X	PI (5 min)	Phalloidin (20 min)	DAPI	Date imaged	Figure #
symbiotic	3	19	2 (half)	12-Oct-22	CTC + DAPI (4hrs)		x		x	x			x		
symbiotic	3	20	1(half)	12-Oct-22	Fixed in 2.5% glut	x			x						
symbiotic	3	20	2 (half)	12-Oct-22	Fixed in 2.5% glut	x			x						
symbiotic	3	20	1(half)	12-Oct-22	Lysotracker + DAPI			x	x	x			x		
symbiotic	3	20	2 (half)	12-Oct-22	CTC + DAPI (4hrs)		x		x	x			x		

Appendix B – Specimen data and experimental maintenance associated with transmission electron micrographs represented in Figures 12 to 14. Specimens labeled "no treatment" were immediately processed for electron microscopy upon collection.

Image #	Specimen ID	Date imaged	Figure	Experiment/Sampling
12954	Control 13	27-Mar-14	12A	Kept in sediment for 4 days
12948	Control 9	27-Mar-14	12B	Kept in sediment for 4 days
12615	TS (2)-6	11-Mar-14	12C	Kept in seawater with 2% thiosulfate for 1 day
12613	TS (2)-6	11-Mar-14	12D	Kept in seawater with 2% thiosulfate for 1 day
12859	TS (2)-3	11-Mar-14	13A	Kept in seawater with 2% thiosulfate for 12 hours
12859	TS (2)-3	11-Mar-14	13B	Kept in seawater with 2% thiosulfate for 12 hours
7985	N-3	24-Jan-13	13C	Collected Jul-12 (no treatment)
7985	N-3	24-Jan-13	13D	Collected Jul-12 (no treatment)
8496	N7-1	21-Feb-13	13E	Collected Oct-12 (no treatment)
8496	N7-1	21-Feb-13	13F	Collected Oct-12 (no treatment)
8453	N-in-S-1.1	14-Feb-13	14A	Starved 40 days (in filtered seawater only), then kept in sediment for 16 days
8454	N-in-S-1.1	14-Feb-13	14B	Starved 40 days (in filtered seawater only), then kept in sediment for 16 days
7270	S6-14	12-Dec-12	14C	Collected May-12 (no treatment)
7270	S6-14	12-Dec-12	14D	Collected May-12 (no treatment)